Neurobiology of Disease

Hyperexcitability and Pharmacological Responsiveness of Cortical Neurons Derived from Human iPSCs Carrying Epilepsy-Associated Sodium Channel Nav1.2-L1342P Genetic Variant

Zhefu Que,[1,2]* Maria I. Olivero-Acosta,[1,2]* Jingliang Zhang,[1,2] Muriel Eaton,[1,2] Anke M. Tukker,[2,3] Xiaoling Chen,[1,2] Jiaxiang Wu,[1,2] Junkai Xie,[5] Tiange Xiao,[1,2] Kyle Wettschurack,[1,2] Layan Yunis,[1,2] J. Marshall Shafer,[1,2] James A. Schaber,[4] Jean-Christophe Rochet,[1,2] Aaron B. Bowman,[2,3] Chongli Yuan,[5] Zhuo Huang,[6] Chang-Deng Hu,[1,7] Darci J. Trader,[1] William C. Skarnes,[8] and Yang Yang[1,2]

[1]Department of Medicinal Chemistry and Molecular Pharmacology, College of Pharmacy, Purdue University, West Lafayette, IN 47907, [2]Purdue Institute for Integrative Neuroscience, Purdue University, Beijing, China, 100191, [3]School of Health Sciences, Purdue University, West Lafayette, IN 47907, [4]Purdue Imaging Facility, Bindley Bioscience Center, Purdue University, West Lafayette, IN 47907, [5]Department of Chemical Engineering, Purdue University, West Lafayette, IN 47907, [6]Department of Molecular and Cellular Pharmacology, School of Pharmaceutical Sciences, Peking University Health Science Center, Beijing, China, 100191, [7]Purdue Center for Cancer Research, Purdue University, West Lafayette, IN 47907, and [8]Cellular Engineering, The Jackson Laboratory for Genomic Medicine, Farmington, CT 06032

With the wide adoption of genomic sequencing in children having seizures, an increasing number of *SCN2A* genetic variants have been revealed as genetic causes of epilepsy. Voltage-gated sodium channel Nav1.2, encoded by gene *SCN2A*, is predominantly expressed in the pyramidal excitatory neurons and supports action potential (AP) firing. One recurrent *SCN2A* genetic variant is L1342P, which was identified in multiple patients with epileptic encephalopathy and intractable seizures. However, the mechanism underlying L1342P-mediated seizures and the pharmacogenetics of this variant in human neurons remain unknown. To understand the core phenotypes of the L1342P variant in human neurons, we took advantage of a reference human-induced pluripotent stem cell (hiPSC) line from a male donor, in which L1342P was introduced by CRISPR/Cas9-mediated genome editing. Using patch-clamping and microelectrode array (MEA) recordings, we revealed that cortical neurons derived from hiPSCs carrying heterozygous L1342P variant have significantly increased intrinsic excitability, higher sodium current density, and enhanced bursting and synchronous network firing, suggesting hyperexcitability phenotypes. Interestingly, L1342P neuronal culture displayed a degree of resistance to the anticonvulsant medication phenytoin, which recapitulated aspects of clinical observation of patients carrying the L1342P variant. In contrast, phrixotoxin-3 (PTx3), a Nav1.2 isoform-specific blocker, can potently alleviate spontaneous and chemically-induced hyperexcitability of neurons carrying the L1342P variant. Our results reveal a possible pathogenic underpinning of Nav1.2-L1342P mediated epileptic seizures and demonstrate the utility of genome-edited hiPSCs as an *in vitro* platform to advance personalized phenotyping and drug discovery.

Key words: **anticonvulsant; epilepsy; hiPSCs; L1342P; SCN2A; voltage-gated sodium channel**

Received Mar. 14, 2021; revised Oct. 10, 2021; accepted Oct. 17, 2021.

Author contributions: Z.Q., M.I.O.-A., and Y.Y. designed research; Z.Q. and M.I.O.-A. performed research; J. X. and W.C.S. contributed unpublished reagents/analytic tools; Z.Q., M.I.O.-A., J.Z., and M.E. analyzed data; Z. Q. wrote the first draft of the paper; Z.Q., M.I.O.-A., J.Z., M.E., A.M.T., X.C., T.X., J.W., K.W., L.Y., J.M.S., J.A.S., J.-C.R., A.B.B., C.Y., Z.H., C.-D.H., D.J.T., and W.C.S. edited the paper; Y.Y. wrote the paper.

This work was also supported by National Institutes of Health National Institute of Neurological Disorders and Stroke (NINDS) Grants R01 NS117585 and R01 NS123154 (to Y.Y.), NINDS Grant R03 NS108229 (to J.-C. R.), National Institute of Environmental Health Sciences Grant R01 ES031401 (to A.B.B), National Cancer Institute Grant R01 CA212403 (to C.-D.H.), and National Institute of Allergy and Infectious Diseases Grant R01 AI150847 (to D.J.T). M.I.O.-A. is supported by the Fulbright-Colciencias Scholarship Program. M.E. is supported by National Science Foundation Graduate Research Fellowship Program Grant DGE-1842166. This work was also supported, in part, by the Indiana Clinical and Translational Sciences Institute, in part by Award Number UL1TR002529 from the National Institutes of Health, National Center for Advancing Translational Sciences, Clinical and Translational Sciences Award. We thank Dr. Amy Brewster for critical reading of this paper and Dr. Lan Chen from the Chemical Genomics Facility of Purdue Institute for Drug Discovery for assay discussion. The also thank support from the Purdue University Institute for Drug Discovery and Institute for Integrative Neuroscience. The Yang lab thanks the *FamilieSCN2A* foundation for the Action Potential Award. Y.Y. was supported by funds from Ralph W. and Grace M. Showalter Research Trust and by Purdue Big Idea Challenge 2.0 on Autism.

* Z.Q. and M.I.O.A contributed equally to this work.

The authors declare no competing financial interests.

Correspondence should be addressed to Yang Yang at yangyang@purdue.edu.

https://doi.org/10.1523/JNEUROSCI.0564-21.2021

Significance Statement

A mounting number of *SCN2A* genetic variants have been identified from patients with epilepsy, but how *SCN2A* variants affect the function of human neurons contributing to seizures is still elusive. This study investigated the functional consequences of a recurring *SCN2A* variant (L1342P) using human iPSC-derived neurons and revealed both intrinsic and network hyperexcitability of neurons carrying a mutant Nav1.2 channel. Importantly, this study recapitulated elements of clinical observations of drug-resistant features of the L1342P variant, and provided a platform for *in vitro* drug testing. Our study sheds light on cellular mechanism of seizures resulting from a recurring Nav1.2 variant, and helps to advance personalized drug discovery to treat patients carrying pathogenic *SCN2A* variant.

Introduction

Epilepsy is a devastating neurologic disease characterized by recurrent episodes of seizures, resulting from the hypersynchronous firing of hyperexcitable neurons that go awry (Jiruska et al., 2013). Affecting ~50 million people worldwide (data from WHO, 2019), its etiology can vary and can be caused by genetic variants (Shorvon, 2011). With the broad adoption of whole-exome sequencing in children with seizures, genetic variants in *SCN2A* have been increasingly identified, emerging as one of the leading genetic causes of epilepsies (Howell et al., 2015; Wolff et al., 2017). *SCN2A*, encoding the α-subunit of the voltage-gated sodium channel Nav1.2, is strongly expressed in principal neurons of the central nervous system, including excitatory glutamatergic neurons of the cortex (Hu et al., 2009; Liao et al., 2010; Tian et al., 2014; Ye et al., 2018). *SCN2A* is responsible for neuronal action potential (AP) initiation, propagation, and backpropagation during different developmental stages (Rush et al., 2005; Spratt et al., 2019). Studies have found "hot spots" in the *SCN2A* sequence, where variants frequently occur (Sanders et al., 2018). In particular, a recurring heterozygous genetic variant (Nav1.2-L1342P variant) has been identified in five patients, sharing similar and distinct features, including epileptic encephalopathy, transient choreoathetotic movements, and hypersomnia, among other symptoms (Hackenberg et al., 2014; Matalon et al., 2014; Dimassi et al., 2016; Li et al., 2016; Wolff et al., 2017). Most of these patients have intractable seizures and are resistant to current medical treatments, which severely impairs their quality of life.

The channel properties of the L1342P variant have been previously studied in human embryonic kidney (HEK293T) cells, revealing profound alterations in gating properties and a mixed gain-loss of function phenotype (Begemann et al., 2019). However, how the L1342P variant affects the function of human neurons is unknown. Technological advances have made the generation of neurons from human-induced pluripotent stem cells (hiPSCs) possible, enabling the study of pathologic features of human neurons carrying disease-associated variants *in vitro* (Liu et al., 2013; Lu et al., 2019; Tidball et al., 2020). While patient-derived hiPSCs are often used for disease modeling, the genetic background of each patient may contribute to the phenotypes independent of the specific genetic mutation of interest. Additionally, when a variant affects more than one patient, it may result in different clinical manifestations. Thus, it would be important to assess the core phenotypes that can be attributed to that variant of interest, which will inform further precision intervention of such recurring variants. To this end, we used a CRISPR/Cas9-mediated genome-editing approach to generate the heterozygous L1342P variant in a well-characterized reference hiPSC line (KOLF2; Kilpinen et al., 2017). The KOLF2 line has publicly available genomic sequencing information, is highly accessible for cross-lab comparison, and has a broad differentiation capacity into different cell types including neurons (Streeter et al., 2017; Siddiqi et al., 2019; Skarnes et al., 2019).

By directly comparing neurons carrying the Nav1.2-L1342P variant with their isogenic wild-type (WT) controls (hereby referred to as "control" in this article), we report that the reference hiPSC-based *in vitro* model clearly shows that the L1342P variant results in hyperexcitability phenotypes in neurons, including strong burst and synchronous firing. Moreover, our *in vitro* platform recapitulates aspects of pharmaco-responsiveness of patients and reveals the efficacy of novel compounds. Our results are likely to inform the development of personalized therapy for epilepsy patients carrying specific genetic variants of *SCN2A*.

Materials and Methods

Transfection of HEK293 cells with SCN2A *plasmid*

The human embryonal kidney cells (HEK293-tsA201 type) were cultured in DMEM media with 10% fetal bovine serum (FBS) and 1% penicillin-streptomycin antibiotics. After reaching 80% confluency, cells were transiently transfected with Lipojet reagent (LipoJet In Vitro Transfection kit, SignaGen Laboratories, catalog #SL100468) to introduce a full-length tetrodotoxin (TTX)-resistant human *SCN2A* control or L1342P variant (gifts from Stephen Waxman, Yale University), in piggyBac vector with a GFP-2A linker, similar to the previously published design (Yang et al., 2016). After 24 h, cells were dissociated into single cells using 0.25% trypsin (Corning, catalog #25-053-CI) and plated on poly-D-lysine-coated coverslips (Corning, catalog #354086) for whole-cell patch-clamp recording.

CRISPR-Cas9 editing of hiPSCs

CRISPR-Cas9 editing of KOLF2-C1 hiPSCs (from male donor) to generate Nav1.2-L1342P heterozygous single-cell derived clones was performed largely as previously described (Skarnes et al., 2019). Briefly, cells were grown in a 5% CO_2, 37°C incubator in StemFlex media (ThermoFisher, catalog #A3349401) on Synthemax-treated wells (Synthemax II; Corning, catalog #3535) and dissociated to single cells with Accutase (Stemcell Technologies, catalog #07920). In a volume of 0.1-ml Primary Cell buffer (Lonza), 1.6×10^6 KOLF2-C1 cells were nucleofected (Lonza Amaxa 4D nucleofector; program CA137) with 20 mg Cas9 protein (HiFi; IDT), 16-mg single guide RNA (the first 20 bases: 5′-ATCTATCATGAATGTACTTC...-3′; chemically-modified; Synthego), and 200 pmol of a 100-mer oligonucleotide repair template (5′-GTTGTAAATGCTCTTTAGGAGCCATTCCATCTATCATGAATGT ACTTCCGGTTTGTCTGATCTTTTGGCTAATATTCAGTATCATGG GAGTGAATCTCT-3′; desalted Ultramer; IDT) containing the L1342P single nucleotide variant. Cas9 ribonucleoprotein complexes were assembled *in vitro* for 30 min before nucleofection. The cells were seeded onto one well of a Synthemax-treated 6-well plate and in StemFlex media containing 1× RevitaCell (ThermoFisher, catalog #A2644501), 30 mM HDR Enhancer (IDT), and cultured at 32°C (cold shock) for 2 d. After 24 h, the media were changed to remove RevitaCell. After 48 h, the media

were changed to StemFlex without HDR Enhancer and cultured to confluency at 37°C. Following the cloning of single-cell derived colonies, genomic DNA was isolated. The target region containing the L1342P SNV was amplified by PCR (0.6-kb amplicon; forward primer, 5′-GGAATTTGATCCCCAAGTGGTCTCT-3′; reverse primer, 5′-AATGAGAGCTTTGCACTCACTGTAG-3′) and subjected to Sanger sequencing (sequencing primer, 5′-TTGGAGCTACCAGAGTCTAG-3′). G-banded karyotyping of the hiPSCs lines was performed using Labcorp's Human Cell Line Authentication Testing Services.

Generation of hiPSC-derived neurons

Cortical neurons were generated with three to four individual differentiations using up to four different hiPSC lines (two for each genotype as "biological replicates") to account for intra-cell line variability. We adopted a modified Dual-SMAD inhibition-based method, which simultaneously inhibits activin/nodal and the bone morphogenetic protein (BMP) signaling pathways with small molecules to drive cells into neuronal fate (Shi et al., 2012b; Boissart et al., 2013; Mehta et al., 2018). In detail, hiPSCs were grown on a Matrigel substrate (Corning, catalog #354230) in StemFlex Medium (ThermoFisher, catalog #A3349401) until 80–90% confluency in a 5% CO_2, 37°C incubator. Colonies were passaged with an EDTA-based dissociation solution, Versene (ThermoFisher, catalog #15040066), and seeded with 10 mM rock inhibitor (RevitaCell Supplement, Invitrogen, catalog #A2644501) for the initial 24 h on ultra-low attachment 96-well plates (Corning, catalog #CLS3474-24EA) with a cell density of 12,000 cells per well to obtain evenly shaped spherical embryoid bodies (EBs). EBs were generated in an EB formation medium containing neural induction medium (Stemcell Technologies, catalog #05835) supplemented with 100 nM LDN-193189 (Sigma, catalog #SML0559) and 10 μM SB431542 (Tocris, catalog #1614). After 7 d, EBs were harvested and replated into rosettes to generate neural progenitor cells (NPCs). A neural rosette selection reagent (Stemcell Technologies, catalog #05832) was used to lift the rosette monolayer and expanded into NPCs. Once neural progenitors were formed, they were plated on poly-L-ornithine (PLO)-laminin-coated coverslips and differentiated for the first 7 d with a formula containing: neurobasal plus medium (Invitrogen, catalog #A3582901), 1× B27 plus supplement (Invitrogen, catalog #A3582801), 1× non-essential amino acids solution (NEAA; Invitrogen, catalog #11140050), and GlutaMAX (Invitrogen, catalog #3505006). Then the medium was switched into a maturation medium for the next 38 d or longer, which contains the following: Brainphys (Stemcell Technologies, catalog #05790), 1× B27 plus supplement (Invitrogen, catalog #A3582801), 1× MEM NEAA (Invitrogen, catalog #11140050), GlutaMAX (Invitrogen, catalog #3505006), 100 μM dibutyryl cAMP (dcAMP; Santa Cruz Biotechnology, catalog #sc-201567A), 200 μM ascorbic acid, 20 ng/ml brain-derived neurotrophic factor (BDNF; ProspecBio, catalog #CYT-207), and 20 ng/ml glial cell-derived neurotrophic factor (GDNF; ProspecBio, catalog #CYT-305). Cell media were replaced every 2–3 d.

Immunocytochemistry

Immunocytochemistry was used to characterize the hiPSCs and determine the fate and maturity of differentiated neurons. Cells were maintained on glass coverslips (Neuvitro, catalog #GG-12-Pre) or 24-well glass-bottom plates with #1.5 cover glass (Celvis, catalog #P24-1.5H-N) previously coated with PLO-Laminin. On the day of the experiment, samples were washed briefly in phosphate-buffered saline (PBS 1×; Corning, catalog #21-040-CMX12) and fixed in 4% paraformaldehyde in PBS at room temperature (RT) for 15 min. Samples were rinsed with PBS three times (5 min for each rinse) and permeabilized for 20 min with 0.3% Triton X-100 (pH 7.4). Samples were blocked with 5% bovine serum albumin (BSA; Sigma catalog #9048) for 1 h at RT, then left to incubate with diluted primary antibodies in 1% BSA in a humidified chamber at 4°C overnight. The next day, samples were rinsed three times with PBS and subjected to fluorescent-dye conjugated Alexa Fluor-based secondary antibodies diluted in 1% BSA for 2 h at RT in the dark. After incubation, the secondary antibody solution was removed, and coverslips were washed three times with PBS (5 min for each wash) in the dark. For DAPI counterstain, VECTASHIELD antifade mounting medium with DAPI (Vector Laboratories, catalog #H-1200) or a PBS-DAPI solution (ThermoFisher, catalog #62238; 1:10,000) was used.

Primary antibodies used for assessment of pluripotency status included a rabbit-anti-octamer-binding transcription factor (OCT4; Cell Signaling Technologies, catalog #C30A3; 1:200) and mouse-anti-Podocalyxin (TRA-1-60; Cell Signaling Technologies, catalog #4796). Mouse-anti Paired box protein Pax-6 (PAX6; Invitrogen, catalog #21103049; 1:300) and rabbit-anti Forkhead box G1 (FOXG1; Abcam, catalog #ab18259; 1:300) were used to stain neural progenitors. Rabbit-anti-β Tubulin III (Abcam, catalog #ab18207; 1:1000), mouse-anti microtubule-associated protein 2 (MAP2; Invitrogen, catalog #13-1500; 1:1000), guinea pig-anti synapsin1/2 (Synaptic Systems, catalog #106044; 1:1000), rabbit-anti vesicular glutamate transporter 1 (VGLUT1; Synaptic Systems, catalog #135302; 1:1000), and CTIP2 (Abcam, catalog #ab18465; 1:300) were used to label hiPSC-derived neurons. Secondary antibodies for both neural progenitors and hiPSC-derived neurons were anti-rabbit or mouse conjugated with Alexa Fluor 488 or Alexa Fluor 555, anti-guinea pig Alexa Fluor 488 and anti-rat Alexa Fluor 647 (Invitrogen; 1:1000). hiPSCs and neuronal cell imaging were acquired with an inverted widefield Nikon Eclipse Ti2 microscope. Images were processed using Nikon Imaging Software Elements (NIS Elements Version 5.02). Representative Z-stack images for NPCs were acquired on a Nikon A1RMP inverted confocal microscope.

Computational modeling

Computational modeling was used to predict the excitability determined by neuronal spiking changes. The numerical simulations were run under the NEURON environment (version 7.72; http://neuron.yale.edu) with a previously established model (Schmidt-Hieber and Bischofberger, 2010; Hallermann et al., 2012). The kinetic parameters of Nav1.2 were modified using a previously reported method according to activation and inactivation variables derived from our experimental data (Ben-Shalom et al., 2017). Other parameters, including neuron physics and ion channel distribution, were in accordance with previous literature. To model the gating kinetics of the L1342P variant, the activation was set to vShift = −6 (vShift = 10 in control and vShift change has an impact on both activation and inactivation). The number of APs was counted during the 20-ms progressively increasing current-injection period, starting from −75-mV membrane potential.

Electrophysiology

Whole-cell patch-clamp recordings were performed with an EPC10 amplifier and Patchmaster v2X90.3 software (HEKA Elektronik) coupled to an inverted microscope (NikonTi-2 Eclipse). For voltage-clamp recording, experiments were conducted at RT with thick-wall borosilicate glass pipettes (BF150-86-10) with open-tip resistances of 2–4 MΩ. The external solution contained the following: 140 mM NaCl, 3 mM KCl, 1 mM $CaCl_2$, 1 mM $MgCl_2$, 10 mM HEPES, and 20 mM dextrose, titrated with NaOH to pH 7.3. The pipette solution contained the following: 140 mM CsF, 10 mM NaCl, 1.1 mM EGTA, 10 mM HEPES, and 20 mM dextrose, titrated with CsOH to pH 7.3. The osmolarity was adjusted with dextrose to 320 mOsm for the extracellular solution and 310 mOsm for the pipette solution. P/N procedure was used to subtract the leak currents. The measurement of the activation of voltage-gated sodium channel was achieved by 10-ms voltage steps from − 80 to + 50 mV with 5-mV increment, with a holding potential of −100 mV. The trace was first fitted with Boltzmann IV (Origin, version 9.7) to obtain the V_{rev} (reverse potential), then the sodium conductance was calculated as $G_{Na} = I_{Na}/(V_m - V_{rev})$, where I_{Na} was the peak current amplitude (relative to the holding potential of −100 mV) under each corresponding voltage step V_m. For steady-state fast inactivation analysis, the value was determined by using 500-ms prepulses to potentials from −140 to −5 mV, followed by a depolarizing test pulse to +5 mV. The window current was calculated as a percentage ratio between the overlapping area and the total area (over the range between −70 and 0 mV) under the activation and inactivation curves. The currents from both control and L1342P variant were recorded at 5 min after obtaining the whole-cell configuration.

For current-clamp recording, thick-wall borosilicate glass pipettes (Sutter Instruments, BF150-86-10) with open-tip resistances of 4–8 MΩ

were pulled, and the same recording system was used. The external solution contained the following: 140 mM NaCl, 3 mM KCl, 2 mM $CaCl_2$, 2 mM $MgCl_2$, 10 mM HEPES, and 15 mM dextrose, titrated with NaOH to pH 7.3; the internal solution contained the following: 140 mM KCl, 3 mM Mg-ATP, 0.5 mM EGTA, 5 mM HEPES, and 20 mM dextrose, titrated with KOH to pH 7.3. Dextrose was added to bring osmolarity to 320 and 310 mOsm for the extracellular and internal solution, respectively. After the cells were matured for 45–50 d, two to three differentiated neurons from each coverslip were recorded. The pyramidal-shaped neurons with multipolar dendrites were selected for electrophysiological recording to ensure consistent sampling. AP properties were analyzed from the first triggered AP in response to a series of depolarizing steps. Rheobase was determined by the minimum current stimulus that can trigger the first AP. The voltage threshold of the spiking waveform was determined at the voltage where dV/dT is >8 mV/ms during the upstroke. The AP amplitude was measured from the peak to the fixed membrane potential of −75 mV. The spike width was determined by measuring the width of the AP when the potential reaches half of the maximum amplitude. The phase-plane plots were generated using the first triggered AP waveform and were superimposed for comparison. The current densities were obtained by normalizing the peak current amplitude to the capacitance. For repetitive firing analysis, the number of AP firings was recorded under each step of graded current injection over the range from 0 to 125 pA in 5-pA increments. The duration of current injection is 400 ms. The input resistance (GΩ) was measured as $(-75\text{-}V_{steady\text{-}state})/20$, where the $V_{steady\text{-}state}$ is the voltage recorded before the end of the −20 pA stimulus.

Microelectrode array (MEA) recordings on hiPSC-derived neurons

Neurons carrying both the Nav1.2-control and heterozygous Nav1.2-L1342P variant were derived (two to three individual preparations from each genotype) from the same protocol (described in the generation of hiPSC-derived neurons) and studied with a procedure as identical as possible to minimize procedure-related variabilities. After 20 d of maturation, neuronal populations were dissociated into single cells using Accutase (Stemcell Technology, catalog #07922), and 100,000 cells in 10 µL suspension were plated on a precoated (PLO) 48-well plate Cytoview plates (Axion, catalog #m768-tMEA-48W) compatible with a Maestro MEA system (Axion Biosystems), with each well containing 16 electrodes. We carefully controlled the seeding density to make sure each well had an equal amount of cells between genotypes or treatment for MEA recording following our published procedure (Yang et al., 2016, 2018; Mis et al., 2019; Verma et al., 2020; Eaton et al., 2021a). Cells were maintained in Brainphys (Stemcell Technology, catalog #05790) medium supplemented with 100 µM dcAMP, 20 ng/ml BDNF, 20 ng/ml GDNF, 200 µM ascorbic acid, and 1× B27 incubated in 37°C for 14 d, with half-volume medium changes two to three times per week. On the day of recording, MEA plates with neurons were stabilized for 5 min in the system (Maestro, Axion Biosystems) in 5% CO_2 at 37°C and a recording was made for 5 min. A total of 200 s of the recording period was taken for analysis. The threshold for determining the voltage spikes was set to greater than six standard deviations from background noise. Active electrodes were defined as more than five spikes per minute of recording, and wells with <25% active electrodes were not included in data analysis. The spike waveforms were continuously monitored to ensure the electrodes were intact and functioning correctly. Synchrony index, bursting frequency, bursting duration, and bursting intensity (spiking frequency within each bursting event) analysis were obtained using the manufacturer software (Neural Metrics Tool, version 2.4. Axion Biosystems). The network synchrony between channels was measured based on the synchrony of spike firing between electrode pairs throughout the whole well (Eggermont, 2006). A burst was defined as a collection of a minimum of five spikes, each separated by an interspike interval (ISI) of <100 ms using the same manufacturer software.

The compound testing was performed using the same 48-well plate during the culture time between 45 and 50 d. The plate was placed on the MEA system for 5 min, followed by a 100-s recording to obtain the baseline measurement. Then, compounds were added to the MEA in a sterile condition, which was followed by another 5-min equilibrium. Afterward, a 100-s recording was made to study the drug effect. Fold changes were calculated by comparing the compound treatment to baseline (for phenytoin and PTx3 baseline inhibition) or kainic acid (KA; for PTx3 inhibition on KA-induced firing). Drugs used were: KA monohydrate (Sigma-Aldrich, catalog #K0250; 5 µM), phrixotoxin-3 (PTx3; R&D Systems, catalog #4914; 15 nM), and phenytoin (Sigma-Aldrich, catalog #PHR1139; 15, 30, 40, 50 µM). Stock solutions of KA and PTx3 were prepared in autoclaved MilliQ water. Stock solutions of phenytoin were made in DMSO (final concentration of DMSO <0.2%).

Statistical analysis

A normality test was performed for all data. Data were analyzed using parametric Student's *t* test, nonparametric Mann–Whitney *U* test, Wilcoxon test, repeated-measures two-way ANOVA or Kruskal–Wallis test depending on the nature of the data (details presented in the result and figure legend) using Origin (OriginLab) and Prism (GraphPad Software). Data are reported as mean ± SEM. The significance threshold was set with $p < 0.05$, with $^{*}p < 0.05$, $^{**}p < 0.01$, and $^{***}p < 0.001$.

Results

Nav1.2-L1342P channel displays complex biophysical properties

The α-subunit of Nav1.2 is comprised of four homologous domains (I to IV), with each domain containing six transmembrane spanning regions (S1–S6). The S1–S4 helices of each domain forms a voltage sensor domain (VSD), and the S5–S6 helical region with an ion selectivity filter forms the pore domain to permit sodium influx (Fig. 1*A*). To visualize the location of the L1342P variant, we used a 3D human Nav1.2 structural model (PDB ID: 6J8E; Fig. 1*B*; Pan et al., 2019). L1342P is positioned at the fifth segment (S5) on Domain III, which is a highly conserved region. The fifth segment and neighboring locations are hotspots for many seizure-related variants (Sanders et al., 2018). L1342P is predicted to disturb interactions with the adjacent S4–S5 linker (Begemann et al., 2019). The structural significance of the S5 region implies that the biophysical properties of Nav1.2 are likely to be profoundly disrupted by the L1342P variant.

To examine the effect of the L1342P variant on the biophysical properties of ion channels, we performed whole-cell voltage-clamp recordings on HEK cells. Two representative whole-cell current traces from cells expressing either control (WT) or Nav1.2-L1342P mutant channels are shown, indicating that functional sodium currents can be recorded from both control and Nav1.2-L1342P channels (Fig. 1*C*). The normalized current versus voltage (I-V) relationship shows a hyperpolarized shift for the L1342P variant (Fig. 1*C*, inset). In particular, the L1342P exhibited a large, hyperpolarized shift of V_{half} in voltage-dependent activation compared with control, suggesting a gain-of-function phenotype (Fig. 1*D*; V_{half} value: control: −19.5 ± 0.5 mV, $n = 9$; L1342P: −35.4 ± 0.5 mV, $n = 11$; $p < 0.001$, Student's *t* test). Steady-state fast inactivation was measured in response to a 500-ms depolarizing potential. L1342P markedly shifted the channel fast-inactivation V_{half} by around 16 mV in the negative direction (V_{half} value: control: −61.6 ± 0.1 mV, $n = 6$; L1342P: −77.8 ± 0.3 mV, $n = 11$; $p < 0.001$, Student's *t* test; Fig. 1*E*), suggesting a loss-of-function attribute. It is worth noting that our results were consistent with a published report, which studied the Nav1.2-L1342P variant in a TTX-sensitive backbone construct together with β1 and β2 subunits in HEK cells (Begemann et al., 2019). Taking channel activation and fast-inactivation together, the L1342P variant resulted in a complex biophysical change at the channel level, showing both gain and loss-of-function phenotypes for different parameters. To further understand the overall

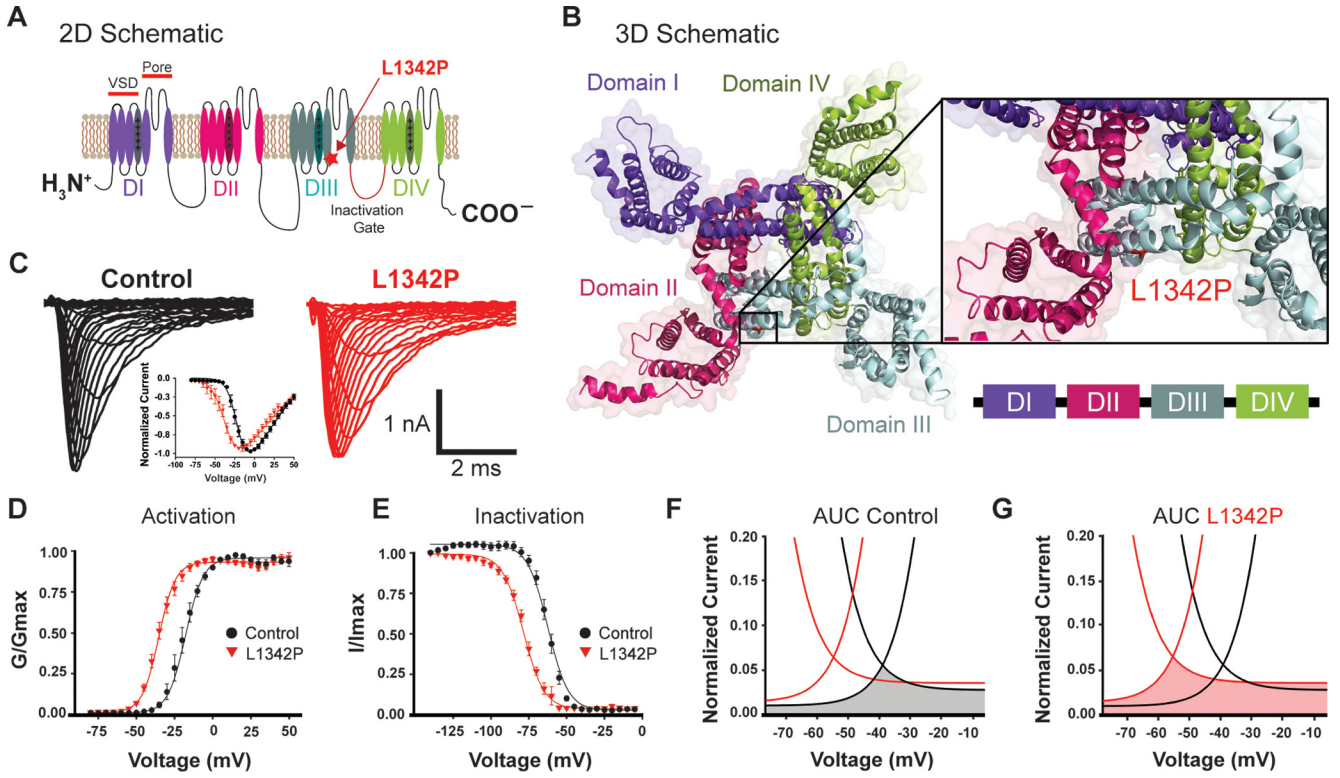

Figure 1. Structural modeling and biophysical properties of the L1342P variant. ***A***, Schematic showing the transmembrane topology of the Nav1.2 sodium channel. Mutated residue L1342P is located at Domain III, in the fifth segment, denoted as a red star. ***B***, Three-dimensional view of a structural model of the Nav1.2 channel's transmembrane domains. The location of the L1342P variant is in the S5 helix of the pore-forming segment. A zoomed-in view is shown on the right. ***C***, Representative traces of whole-cell sodium current from HEK cells expressing control Nav1.2 (left) or Nav1.2-L1342P channel (right). The inset in panel ***C*** depicts the normalized I-V curve. ***D***, Voltage-dependent activation. The normalized conductance was plotted against the voltage of a series the test pulses, ranging from –80 to 50 mV, and then fitted with the Boltzmann equation. ***E***, Steady-state fast inactivation of control and L1342P mutant channels. The relationship between the normalized current peak amplitude and prepulse potential was plotted and fitted with the Boltzmann function. ***F***, ***G***, Illustrative presentation of window current analysis for control (***F***) and L1342P (***G***). The shaded area depicts window current, which is the overlapping region under the activation and inactivation curves.

effect of these biophysical changes, we calculated the window current. Window current is defined as the inward current that arises from partial activation and incomplete inactivation of the sodium channel, the magnitude of which can be used to assess the net effect of gain-of function versus loss-of-function of a particular variant (Patlak, 1991; Berecki et al., 2018). Our calculation revealed that the magnitude of the window current from L1342P was not significantly changed from control (control: I_{Na}/total = 5.2 ± 0.8%; L1342P: I_{Na}/total = 6.3 ± 0.9%, $p = 0.38$, Student's t test; Fig. 1*F*,*G*). Thus, our data show that biophysical analysis alone is not likely to provide a clear-cut answer regarding gain-of function versus loss-of function features of the L1342P variant.

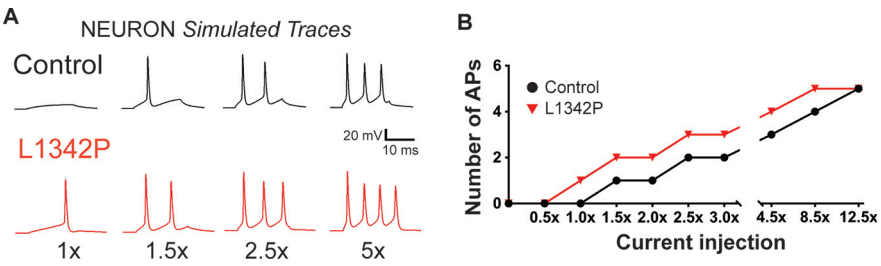

Figure 2. Single-compartment simulation in a virtual neuron with the Nav1.2-L1342P variant predicts a gain-of-function phenotype. ***A***, Computational simulation predicted a higher firing frequency in the virtual neuron model with the L1342P variant. The stimulus duration is 20 ms. ***B***, The input-output relationship showed a significantly increased number of spikes in the range of current injections for the L1342P variant.

Single-compartment simulation predicts a gain-of-function phenotype in a pyramidal neuron model with the Nav1.2-L1342P variant

To further study how the L1342P variant of Nav1.2 alters neuronal excitability, we used the NEURON simulation to model the firing properties of pyramidal neurons, in which Nav1.2 is strongly expressed (Hu et al., 2009; Liao et al., 2010; Tian et al., 2014; Ye et al., 2018). Modeled with the biophysical properties measured in our HEK293 cell study, we found that a simulated neuron with Nav1.2-L1342P is notably more excitable. We define the minimal current injected to elicit the AP firing of neurons modeled with L1342P as 1×. This same 1× current injection, however, cannot trigger AP firing in neurons modeled with control Nav1.2 channel (Fig. 2*A*). The number of APs from neurons modeled with Nav1.2-L1342P increases in response to elevated current injection. At each current injection level, neurons modeled with Nav1.2-L1342P had more AP firing than neurons modeled with control Nav1.2 channel over a broad range of current injections (Fig. 2*B*). Collectively, our results from computational modeling suggest an overall hyperexcitability phenotype in neurons carrying the Nav1.2-L1342P variant, which prompts us to test this prediction in human neuron-based models.

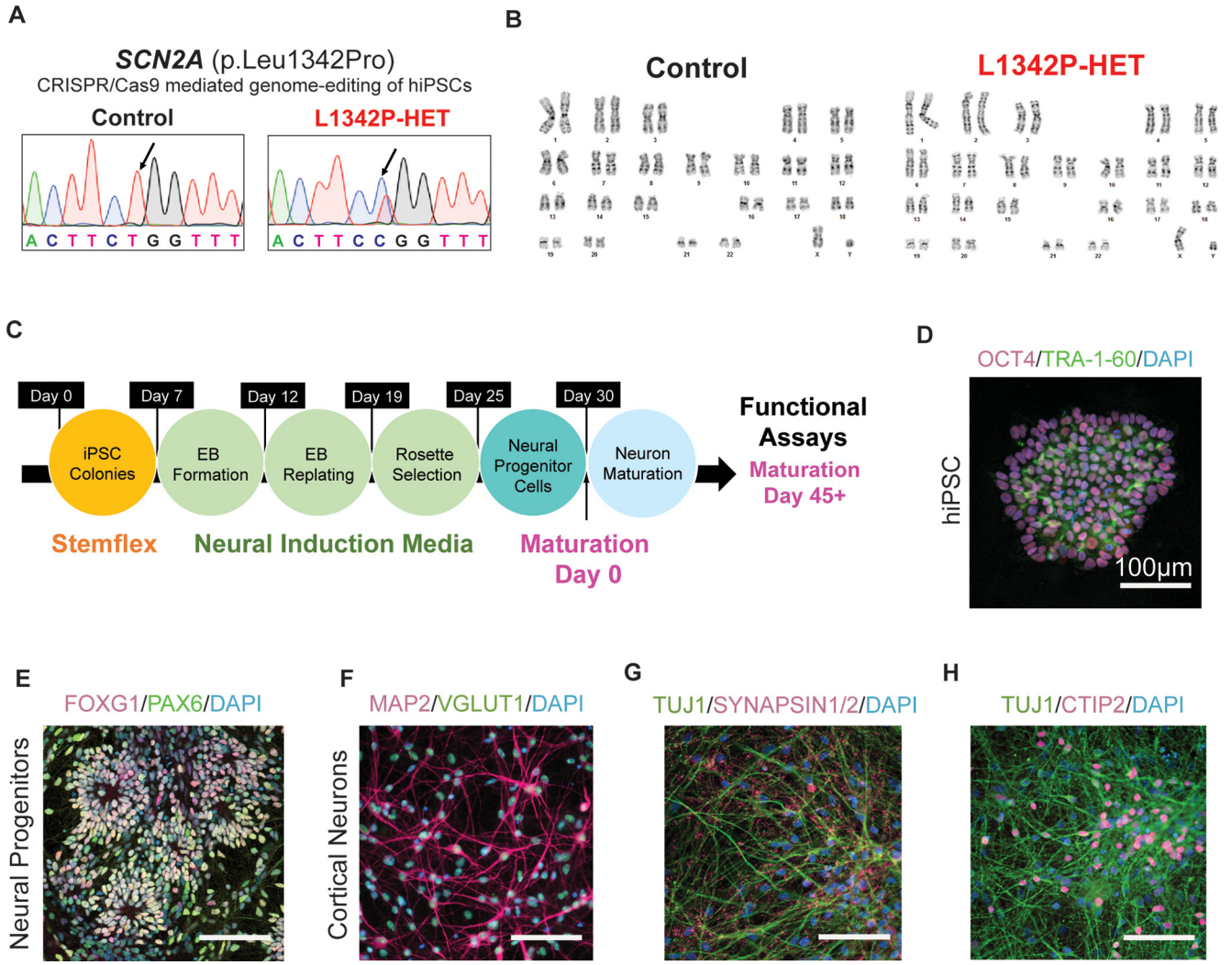

Figure 3. Characterization of hiPSC-derived neurons reveals a cortical neuron fate. ***A***, Sequencing of Nav1.2 DNA from isogenic control (black) and Nav1.2-L1342P (red) hiPSCs after CRISPR/Cas9-mediated genome editing. ***B***, Representative karyotype analysis shows normal diploid 46XY karyotypes for both control and L1342P iPSCs lines. ***C***, Schematic of a modified DUAL-SMADi differentiation protocol and the timeline for experiments. ***D***, Immunofluorescence staining of control hiPSCs with pluripotency markers OCT4 and TRA-1-60. ***E***, Staining of neural progenitors with markers including FOXG1 and PAX6 (dorsal forebrain markers). ***F***, Immunofluorescence image of control hiPSC-derived glutamatergic neurons expressing MAP2, colocalized with VGLUT1. ***G***, Colocalized expression of TUJ1 and synapsin1/2 was seen in the neuronal culture, suggesting that synaptic connectivity was formed among neurons. ***H***, Cortical layer marker CTIP2 indicates the cortical identity of hiPSC-derived neurons. DAPI was used to stain nuclei.

hiPSCs carrying the L1342P variant can be differentiated into a cortical glutamatergic neuronal fate

Excitatory glutamatergic neurons in the cortex are a key cell type involved in seizures (Howell et al., 2015; Ben-Shalom et al., 2017) and the methodology to reliably generate cortical glutamatergic neurons from hiPSCs is well established (Deneault et al., 2019; Ghatak et al., 2019; Quraishi et al., 2019). To understand how the Nav1.2-L1342P variant affects the function of human cortical neurons, we used CRISPR/Cas9 to recapitulate the sequence change of heterozygous Nav1.2-L1342P in a reference hiPSC (KOLF2) line (referred to as L1342P thereafter; Skarnes et al., 2019). The Nav1.2-L1342P variant has been identified from multiple patients with both shared and distinct phenotypes (Hackenberg et al., 2014; Matalon et al., 2014; Dimassi et al., 2016; Li et al., 2016; Wolff et al., 2017). Thus, a reference hiPSC line has the advantage of reducing the influence of the genetic background across individual patients and allowed us to assess the core impact of the Nav1.2-L1342P variant on neuronal functions compared with isogenic controls.

After CRISPR/Cas9-mediated editing, we successfully obtained both isogenic control and heterozygous L1342P hiPSCs validated by sequencing (Fig. 3*A*). To address potential CRISPR off-target effects, we sequenced the two sites that share the greatest sequence similarity (two mismatches) with our target site (genome analysis revealed only two sites with two mismatches in the guide RNA within the whole genome). Our sequencing results showed that there was no off-target damage in genomic sites that have the closest similarity. To evaluate the genomic integrity of cell lines undergoing the gene-editing, we performed a karyotype analysis. The analysis revealed a normal 46XY karyotype (Fig. 3*B*). Then hiPSCs were differentiated into glutamatergic cortical neurons using an established protocol (Fig. 3*C*). Undifferentiated hiPSC colonies displayed normal and homogenous morphology with defined edges and low levels of spontaneous differentiation. They consistently expressed pluripotency markers, including OCT4 and TRA-1-60 (Fig. 3*D*). When we differentiated these hiPSCs into NPCs, we identified high proportions of dorsal telencephalic neuroepithelial markers PAX6 and FOXG1, supporting the forebrain identity of the NPCs (Fig. 3*E*).

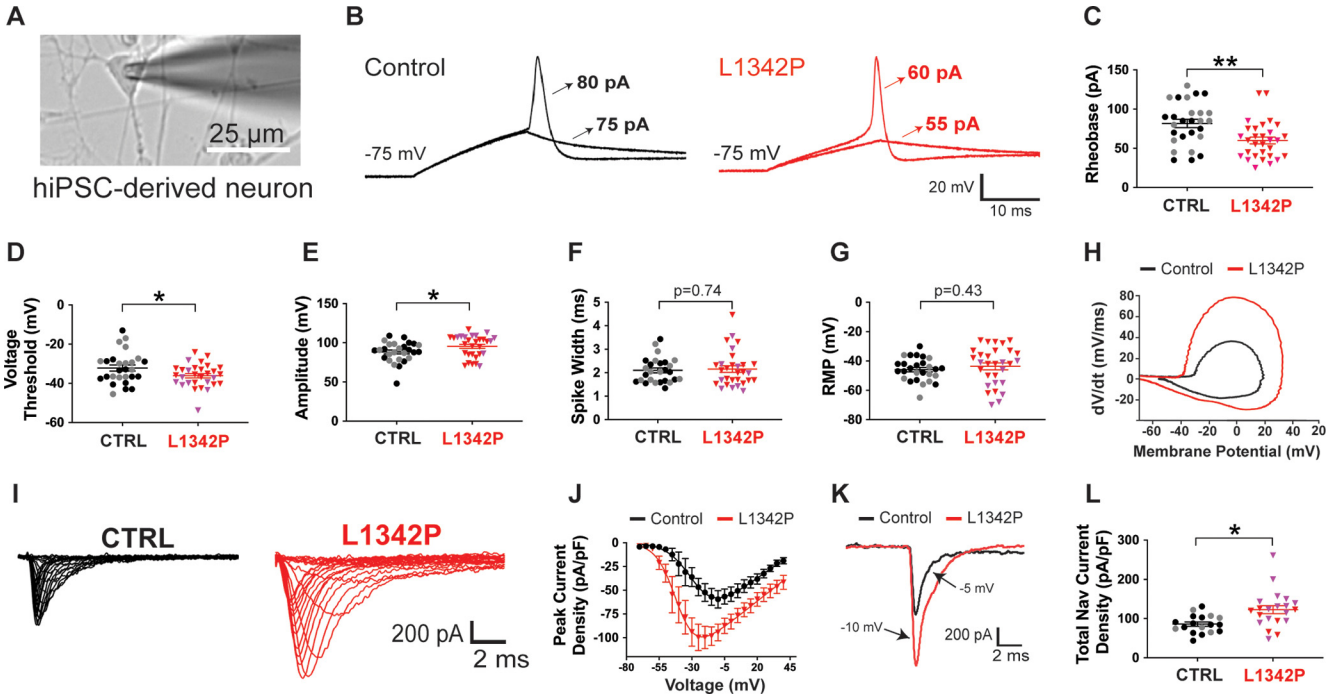

Figure 4. The L1342P variant increases the intrinsic excitability of hiPSC-derived neurons. ***A***, Representative brightfield image of a hiPSC-derived pyramidal-shaped neuron selected for patch-clamp experiments. ***B***, Representative single AP triggered by a stepwise increment of current stimulus with a 20-ms duration. There is a difference in the rheobase of firing between isogenic control and L1342P neurons at a fixed membrane potential of −75 mV. The current threshold of the representative neurons shown here was 80 pA for isogenic control neuron, and 60 pA for L1342P neuron. ***C***, The L1342P variant reduced the minimal current needed for evoking an intact AP in neurons. ***D***, The voltage threshold of AP was hyperpolarized in L1342P neurons. ***E***, APs from neurons carrying the L1342P variant had an elevated peak amplitude. ***F***, The L1342P variant did not change the width of the AP. ***G***, Resting membrane potentials were not changed between control and L1342P neurons. ***H***, Representative phase plot of APs for control (black) and L1342P (red) neuron. ***I***, Representative families of sodium current traces for isogenic control and L1342P neuron (outward current was blocked using the tetraethylammonium chloride in bath solution). ***J***, Averaged peak current density versus voltage relationship (activation V_{half} of control −27.7 ± 3.1 mV vs activation V_{half} of L1342P: −40.9 ± 2.0 mV, $p = 0.02$). ***K***, Representative sodium current traces for control and L1342P neuron. Sample traces were plotted under −5 and −10 mV. ***L***, The total sodium current density was significantly increased in L1342P neurons. The total current density is the maximum current obtained from a family of sodium currents in an individual neuron. Note that the peak sodium current from each individual neuron may come from different steps of voltage command. Data were collected from four independent differentiated batches with two clones (showed with two different colors) used from each genotype. Data were analyzed by Student's *t* test; $*p < 0.05$, $**p < 0.01$.

After 45 d of maturation, differentiated cortical neurons displayed a pyramidal shape with neurites and expressed mature neuron-specific markers. MAP2 and βIII-tubulin staining was found in both soma and processes (neurites), consistent with the literature (Fig. 3*F–H*; Shi et al., 2012a; Kouroupi et al., 2017; Mehta et al., 2018; Satir et al., 2020). Moreover, we found that the vast majority of hiPSCs-derived cortical neurons expressed VGLUT1 (control: 93.60 ± 0.66%, $n = 26$ fields of view across three cultures; L1342P: 90.38 ± 1.50%, $n = 30$ fields of view across three cultures; $p = 0.11$), indicating an abundant presence of glutamatergic neurons (Fig. 3*F*). To determine the structural maturity of neurons, presynaptic proteins synapsin 1 and 2 (SYN1/2) were studied, which were revealed to be distributed along the axons in dotted patterns, indicating the formation of connectivity (Fig. 3*G*). Expression of the cortical marker CTIP2 was also evident in the cultures, indicating cortical characteristics (Fig. 3*H*). Together, these data provide evidence that the CRISPR-engineered hiPSCs carrying Nav1.2-L1342P and their corresponding isogenic control can be differentiated into cortical glutamatergic neurons.

Intrinsic excitability is enhanced in hiPSC-derived neurons carrying the Nav1.2-L1342P variant

Our results from computational modeling and whole-cell voltage-clamp recordings suggested that neurons carrying the Nav1.2-L1342P variant are likely to display a gain-of-function phenotype. To directly test this hypothesis, we used cortical neurons derived from hiPSCs to examine the functional consequences of the Nav1.2-L1342P variant. After 45-50 d of maturation, pyramidal-shaped neurons were selected for whole-cell current-clamp experiments (Fig. 4*A*). Neurons were held at a fixed −75-mV membrane potential, and we progressively depolarized the neurons by intracellular current injections from 0 to 125 pA, with a step of 5-pA increment. We found that the isogenic control neuron did not fire an AP until the injected current reached 80 pA, which was defined as the rheobase. In contrast, an L1342P neuron started to fire with a lower current injection of 60 pA (Fig. 4*B*). Quantitatively, we found a 25% reduction in rheobase of L1342P neurons, statistically different from isogenic control neurons (control: 81.7 ± 5.3 pA, $n = 27$; L1342P: 60.0 ± 4.3 pA, $n = 30$; $p = 0.002$, Student's *t* test; Fig. 4*C*). We further analyzed the voltage threshold of spiking since it is likely to be influenced by sodium channel dysfunctions (Ye et al., 2018). Our results revealed that L1342P neurons had a significantly lower voltage threshold, which indicates a higher probability to fire under a more hyperpolarized membrane potential (control: −32.2 ± 1.5 mV, $n = 27$; L1342P: −36.2 ± 1.1 mV, $n = 30$; $p = 0.04$, Student's *t* test; Fig. 4*D*). Furthermore, we found that the amplitude of AP was significantly enhanced in L1342P neurons, with an average amplitude ~7 mV larger than that of isogenic control (control: 88.3 ± 2.5 mV, $n = 27$; L1342P: 95.4 ± 2.5 mV, $n = 30$; $p = 0.04$, Student's *t* test; Fig. 4*E*). On the other hand, we found no statistically significant difference in AP (spike) width (control: 2.1 ± 0.1, $n = 27$; L1342P: 2.2 ± 0.1, $n = 30$; $p = 0.74$, Student's *t*

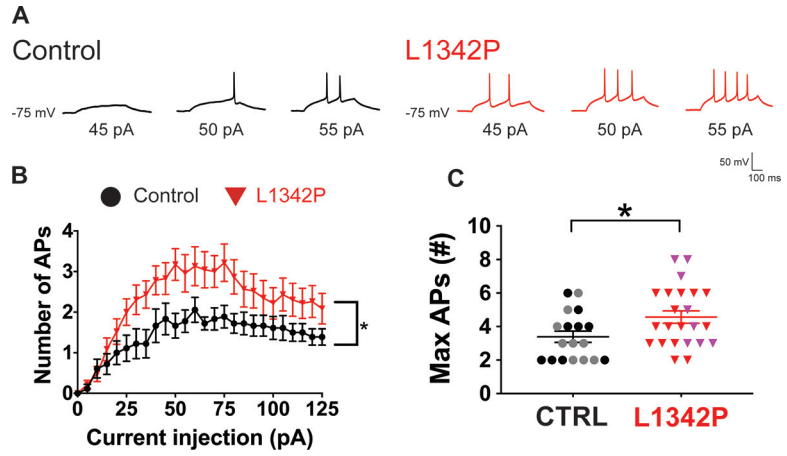

Figure 5. The L1342P variant enhances the repetitive firing of hiPSC-derived neurons. ***A***, Representative sustained AP firings from hiPSC-derived Nav1.2-L1342P (red) cortical neurons or isogenic control (black). ***B***, Plot showing AP number per epoch in response to graded inputs from 0- to 125-pA current injection (400-ms duration). L1342P neurons consistently fired more APs than isogenic control neurons. ***C***, Maximum number of APs triggered from each neuron under the range of 0- to 125-pA current injections. Data were collected from four independent differentiated batches, with two clones (represented by two colors) used for each genotype. Data in ***B*** were analyzed by repeated-measures two-way ANOVA analysis, and data in ***C*** were analyzed by Student's *t* test; $^*p < 0.05$.

test; Fig. 4*F*) between the isogenic control and L1342P neurons. Next, we measured the resting membrane potential to see whether L1342P variant can alter this property. However, we found the resting membrane potential was largely unchanged (control: -45.9 ± 1.5 mV, $n = 27$; L1342P: -43.7 ± 2.4 mV, $n = 30$; $p = 0.43$, Student's *t* test; Fig. 4*G*). To evaluate overall changes in single AP waveforms, phase plane plots were constructed from the first derivative of the membrane potential (dV/dt) versus the membrane potential. We found a lower AP threshold, with a larger peak amplitude and maximum value of dV/dt, in the L1342P neuron (Fig. 4*H*). Collectively, our data indicates that the L1342P variant allows neurons to fire APs more easily, making the neurons intrinsically more excitable.

Our experiments on the channels' biophysical properties revealed a profound shift in channel activation, but whether the finding we observed in HEK cells may be recapitulated in hiPSC derived neurons was not known. Additionally, the literature suggested that sodium channel variants might affect the channel trafficking and membrane expression to increase current density, contributing to neuronal hyperexcitability (Rusconi et al., 2007; Misra et al., 2008; Thompson et al., 2020). However, whether the L1342P variant might affect neuronal excitability in such a manner was not known either. To address these questions, we recorded families of voltage-dependent inward current traces from hiPSC-derived neurons carrying control or L1342P mutant channels in the voltage-clamping configuration (Fig. 4*I*). Interestingly, we found that the hyperpolarized activation shift in the Nav1.2-L1342P channel expressed in HEK cells was partially recapitulated in hiPSC-derived neurons (V_{half} of control -27.7 ± 3.1 mV vs V_{half} of L1342P: -40.9 ± 2.0 mV, $p = 0.02$, Student's *t* test; Fig. 4*J*). While it is worth noting that besides Nav1.2, hiPSC-derived cortical neurons could express additional sodium channels isoforms (e.g., Nav1.3 and Nav1.6), we observed a significantly increased sodium current density in these neurons carrying Nav1.2-L1342P variant (control: 85.9 ± 5.4 pF/pA, $n = 18$; L1342P: 122.9 ± 10.3 pF/pA, $n = 21$; $p = 0.003$, Student's *t* test; Fig. 4*K*,*L*). This increased sodium current density, however, is not accompanied by a change in cell capacitance (control: 18.7 ± 1.5 pF, $n = 18$; L1342P: 22.0 ± 2.7 pF, $n = 21$; $p = 0.30$, Student's *t* test). A higher current density of sodium channel and hyperpolarized shift in activation, together with reduced rheobase and voltage threshold, are likely to serve as the basis underlying the increased intrinsic excitability of neurons carrying the L1342P variant.

Repetitive firing is elevated in hiPSC-derived neurons carrying the Nav1.2-L1342P variant

To further investigate how the L1342P variant affects repetitive AP firings, we performed whole-cell current-clamp recording to study triggered firing. Our data revealed a major difference of repetitive firing between neurons carrying L1342P variant compared with isogenic controls using a prolonged 400-ms current stimulus ranging from 0 to 125 pA in 5-pA increments. From the 45- to 55-pA stimulus, L1342P neuron fired two to four APs in response to current steps (Fig. 5*A*, right panel). In contrast, single or at most two APs were elicited in isogenic control neurons (Fig. 5*A*, left panel). Overall, the L1342P neurons fired significantly more APs than the isogenic controls in the range of 0–125 pA (repeated-measures two-way ANOVA analysis, $F_{(1,39)} = 6.67$, $p = 0.014$; Fig. 5*B*). It is worth noting that we also observed a distinct pattern from the input-output relationship of isogenic control and L1342P neurons. Under depolarizing current within 0–20 pA, the firing frequencies elicited between two groups in each step is similar. Starting from 20 pA, we observed a steeper slope of increase in firing from the L1342P neurons until the 75-pA current injection, indicating that they are more responsive to the stimulus during this range. However, the curve from L1342P neurons fell between the range of 75–125 pA, while isogenic control neurons retained a steady firing frequency after achieving the plateau. Importantly, the maximum number of AP firings that could be triggered by current injection was significantly higher in L1342P neurons, showing a 35% increase over control neurons (control: 3.4 ± 0.3, $n = 18$; L1342P: 4.6 ± 0.4, $n = 23$; $p = 0.02$, Student's *t* test; Fig. 5*C*). We then compared the input resistance and found no significant difference between the control and L1342P neurons (control: 2.0 ± 0.2 pF, $n = 18$; L1342P: 1.6 ± 0.2 pF, $n = 23$; $p = 0.16$, Student's *t* test). While a potassium chloride-based solution (we used herein) is widely used to study neurons (Parker et al., 2018; Mis et al., 2019; Halliwell et al., 2021), it may depolarize the cell membrane. To address the potential issue that the potassium chloride in the internal solution may change the firing property, we performed an additional experiment by using a potassium acetate-based solution. Consistently, we found that the L1342P neurons fired more APs over the whole range (0–125 pA) of current injections in the recording with potassium acetate ($n = 6$ for control neurons and $n = 7$ for L1342P neurons. Repeated-measures two-way ANOVA analysis, $F_{(1,11)} = 6.15$, $p = 0.03$). Together, our data suggest that the L1342P variant greatly influences repetitive firing, leading to a hyperexcitability phenotype of neurons.

Neural network excitability is heightened in hiPSC-derived neurons carrying the Nav1.2-L1342P variant

We observed elevated evoked AP firing of individual neurons carrying the Nav1.2-L1342P variant in our single-cell patch-clamp recording. However, whether this enhanced intrinsic

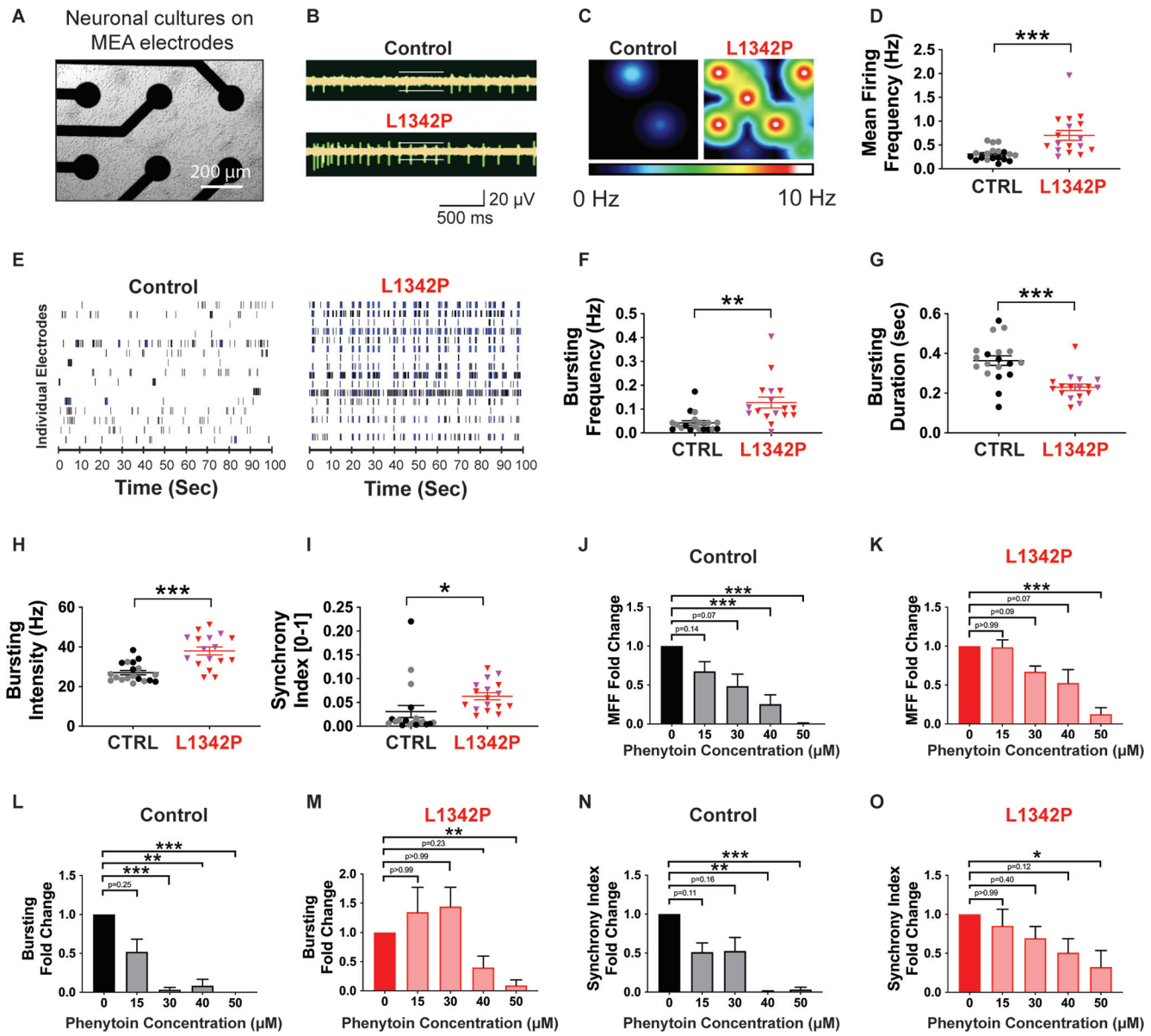

Figure 6. Elevated network excitability revealed by MEA recordings of hiPSC-derived neurons carrying the L1342P variant. ***A***, MEA well plated with hiPSC-derived neurons. ***B***, Representative raw spikes from isogenic control and L1342P cultures. Each spike indicated a spontaneous activity event. ***C***, Heat map of neuronal firing. The intensity of firing frequency is color coded, with warm colors (white, red, orange, and yellow) indicating high firing frequency and cool colors (green and blue) depicting low firing frequency. Each color circle represents an active electrode. ***D***, Mean firing frequency (MFF) comparison between isogenic control and L1342P cultures. ***E***, Representative spike raster plots generated for isogenic control and Nav1.2-L1342P cultures. Each row represents the spikes recorded from one electrode across 100 s, with each tick indicating a spontaneous event. Bursting events are depicted by a cluster of ticks in blue. ***F–I***, Parameters quantitatively describing the network activities in neuron culture, including bursting frequency (***F***), bursting duration (***G***), bursting intensity (***H***), and synchrony index (***I***). Data were pooled from wells across four hiPSC lines (two for each genotype with two differentiations), with $n = 19$ (wells) for isogenic control and $n = 17$ (wells) for the L1342P culture. Four different MEA plates were used in total. The Student's *t* test was performed when data were normally distributed (Kolmogorov–Smirnov normality test), and Mann–Whitney *U* was performed when data were not normally distributed; $^{*}p < 0.05$, $^{**}p < 0.01$. ***J–O***, Inhibitory effects of different doses of phenytoin for isogenic control (***J***, ***L***, ***N***) and L1342P cultures (***K***, ***M***, ***O***). Data are presented as a fold change of MFF, bursting frequency, or synchrony index in response to increasing concentrations of phenytoin from 15 to 50 μM. The neuron cultures for drug testing were pooled from two differentiations, and the sample size was $n = 7, 8, 6, 6$ (wells) for different drug concentrations in control cultures, and $n = 6, 6, 6, 8$ (wells) for L1342P cultures. Kruskal–Wallis test was performed with Dunn's multiple comparisons *post hoc* analysis; $^{*}p < 0.05$, $^{**}p < 0.01$, $^{***}p < 0.001$.

excitability translates into higher activities in a neural network is unknown. MEA is a relatively high-throughput extracellular recording assay that can record the firing of a population of neurons in their standard culture medium, providing a physiologically relevant avenue to assess neuronal network excitability (Fig. 6*A*; Yang et al., 2016, 2018; Mis et al., 2019).

Spontaneous neuronal network activity was recorded using MEA, which showed that the L1342P neuron culture fired at a higher level than the isogenic control culture in traces of a 2.5-s epoch (Fig. 6*B*). The firing of a population of neurons can be visualized in a heat-map view. Each colored circle represented an active electrode (Fig. 6*C*), with blue suggesting low firing frequency and yellow/red indicating high firing frequency. In a representative isogenic control culture, two active electrodes exhibited low activity, whereas the L1342P culture had five active electrodes with higher activity (Fig. 6*C*). Quantitatively, MEA recordings revealed that the mean firing frequency (MFF) of L1342P cultures were substantially elevated compared with

isogenic control cultures (control: 0.31 ± 0.03 Hz, $n = 19$; L1342P: 0.70 ± 0.1 Hz, $n = 17$; $p < 0.001$, Student's t test; Fig. 6*D*). To further understand the temporal firing activity of these neurons, we analyzed the raster plots of the MEA recording, in which the recorded activity of each electrode was plotted over time. While we observed a similar number of active electrodes across wells, we detected more bursting events in L1342P neuron cultures compared with isogenic control culture (Fig. 6*E*). In isogenic control cultures, the active electrodes were firing at a relatively low frequency with scattered firing characteristics over 100 s. In contrast, the representative well-wide raster plot of L1342P cultures showed a higher firing rate with notable bursting events over the same recording window (Fig. 6*E*).

Bursting events, including the bursting frequency, bursting duration, and bursting intensity (spiking frequency within each bursting event), were further quantified as these are seizure-related firing characteristics of neuronal cultures (Fruscione et al., 2018; Tukker et al., 2018, 2020b; Quraishi et al., 2019). The bursting frequency was significantly increased in L1342P cultures compared with isogenic control cultures (control: 0.04 ± 0.009 Hz, $n = 19$; L1342P: 0.13 ± 0.02 Hz, $n = 17$; $p = 0.0002$, Mann–Whitney U; Fig. 6*F*). Interestingly, while the bursting duration was shortened significantly in L1342P cultures (control: 0.36 ± 0.02 s, $n = 19$; L1342P: 0.23 ± 0.02 s, $n = 17$; $p < 0.0001$, Student's t test; Fig. 6*G*), the bursting intensity was markedly elevated, which was reflected by the decreased ISI within the burst (control: 27 ± 1.1 Hz, $n = 19$; L1342P: 38 ± 2.0 Hz, $n = 17$; $p < 0.0001$, Student's t test; Fig. 6*H*). Furthermore, we measured the synchrony index, which was determined by the synchrony of spike firing between electrode pairs (Eggermont, 2006), to reflect the strength of synchronized activities between neurons (value is between 0–1, with 1 indicating the highest synchrony). The synchrony index was markedly increased in L1342P neuron cultures (Fig. 6*I*), suggesting seizure-related hypersynchronization (control: 0.03 ± 0.01, $n = 19$; L1342P: 0.06 ± 0.01, $n = 17$; $p = 0.04$, Mann–Whitney U).

To rule out the possibility that the changes we observed in MEA recordings may come from the differences in cell survivability between groups, we performed a cell viability assay using a NUCLEAR-ID Blue/Red cell viability reagent (Enzo Life Sciences). We observed that the majority of control neurons and L1342P neurons were viable without major differences in viability or density, and the number of neurons was comparable between groups (control: 95.3 ± 0.5%; L1342P: 95.9 ± 0.5%, $p = 0.38$; $n = 4$ wells). Therefore, cell viability/density is not likely to contribute to the changes in the numbers of active neurons and firing frequencies that was observed in the MEA experiments. In conclusion, the results in MEA are consistent with the observation of enhanced intrinsic excitability of L1342P neuron culture in patch-clamping recording while further demonstrate elevated network excitability, including bursting and synchronous firing caused by the L1342P variant.

Sensitivity toward the anticonvulsant phenytoin is reduced in hiPSC-derived neurons carrying the Nav1.2-L1342P variant

In clinical observations, patients carrying the Nav1.2-L1342P variant develop intractable seizures with a minimal response toward commonly used antiepileptic drugs (AEDs; Hackenberg et al., 2014). To test whether we could recapitulate elements of this clinical observation in a cell-based model, we studied a commonly used first-line anticonvulsant phenytoin using the MEA platform. Phenytoin is a general sodium channel blocker and has been shown to inhibit high-frequency repetitive spikings characteristic of seizure episodes (Boerma et al., 2016; Braakman et al., 2017; Gorman and King, 2017; Gardella et al., 2018). We found that in isogenic control cultures, a reduction in the mean firing rate was detectable on treatment with phenytoin at concentrations as low as 15 μM phenytoin, and a statistically significant reduction was evident at a phenytoin concentration of 40 μM (Kruskal–Wallis with Dunn's *post hoc* test, $p = 0.14$, $p = 0.07$, $p = 0.001$, and $p < 0.0001$ for each group comparing with baseline; Fig. 6*J*). However, 15 μM phenytoin did not reduce the mean firing rate of L1342P cultures at all, and 50 μM of phenytoin was required to achieve a statistically significant reduction of mean firing rate in L1342P culture (Kruskal–Wallis with Dunn's *post hoc* test, $p > 0.99$, $p = 0.09$, $p = 0.07$, and $p < 0.0001$ for each group comparing with baseline; Fig. 6*K*). Interestingly, similar trends were also observed for measures of bursting and synchrony. In control cultures, a low dose (30 μM) of phenytoin was able to reduce the bursting significantly (Kruskal–Wallis with Dunn's *post hoc* test, $p = 0.25$, $p = 0.0002$, $p = 0.001$, and $p = 0.0002$ for each group comparing with baseline; Fig. 6*L*), but for L1342P cultures, a significant difference was not achieved until the concentration of phenytoin reached 50 μM (Kruskal–Wallis with Dunn's *post hoc* test, $p > 0.99$, $p > 0.99$, $p = 0.23$, and $p = 0.006$ for each group comparing with baseline; Fig. 6*M*). The synchrony index also showed a difference in the level of reduction in a dose-dependent manner between control and L1342P cultures. We found that a phenytoin concentration of 15–30 μM was effective in reducing the synchronized firing, and almost reduced it to zero when the concentration reached 40 μM or more for control cultures (Kruskal–Wallis with Dunn's *post hoc* test, $p = 0.11$, $p = 0.16$, $p = 0.004$, and $p = 0.0004$ for each group comparing with baseline; Fig. 6*N*). However, in L1342P cultures, while the synchrony index showed a trend of dropping progressively in response to an increasing dose of phenytoin, no significant difference was observed until the concentration reached 50 μM (Kruskal–Wallis with Dunn's *post hoc* test, $p > 0.99$, $p = 0.40$, $p = 0.12$, and $p = 0.01$ for each group comparing with baseline; Fig. 6*O*). Our data thus suggest that neurons carrying the L1342P variant are likely to have a reduced sensitivity toward phenytoin, providing a plausible explanation for the clinical observation that patients carrying the Nav1.2-L1342P variant are largely resistant to this commonly prescribed therapy.

The Nav1.2-specific inhibitor PTx3 reduces the spontaneous and chemically-induced firing of hiPSC-derived neurons carrying the Nav1.2-L1342P variant

General sodium channel blockers (e.g., phenytoin) have limited efficacy for many patients with a variety of sodium channel variants (Boerma et al., 2016; Syrbe et al., 2016; Braakman et al., 2017; Wolff et al., 2017). Therefore, the development of isoform-specific blockers to treat patients carrying sodium channel variants in a precision medicine manner is desirable. Although Nav1.6-specific and Nav1.6/Nav1.2 dual-specificity blockers have been reported (Bialer et al., 2018), isoform-specific blockers for Nav1.2 are not currently available. Neurotoxin PTx3 has been suggested as a Nav1.2-specific blocker when used at a dose at or below 30 nM (Li et al., 2014; Yin et al., 2017; Risner et al., 2020). While PTx3, as a neurotoxin, may not be directly useful in a clinical setting, we nevertheless studied the inhibitory effect of PTx3 on our neuronal cultures to provide proof-of-concept evidence of the utility of Nav1.2-specific blocker for clinical translation. We first validated the effect of 10 nM PTx3 in control hiPSC-derived neurons and found that the peak current was reduced significantly (10 nM PTx3: 78.3 ± 4.1% compared with baseline, $p = 0.0002$, Student's t test). This result also confirmed

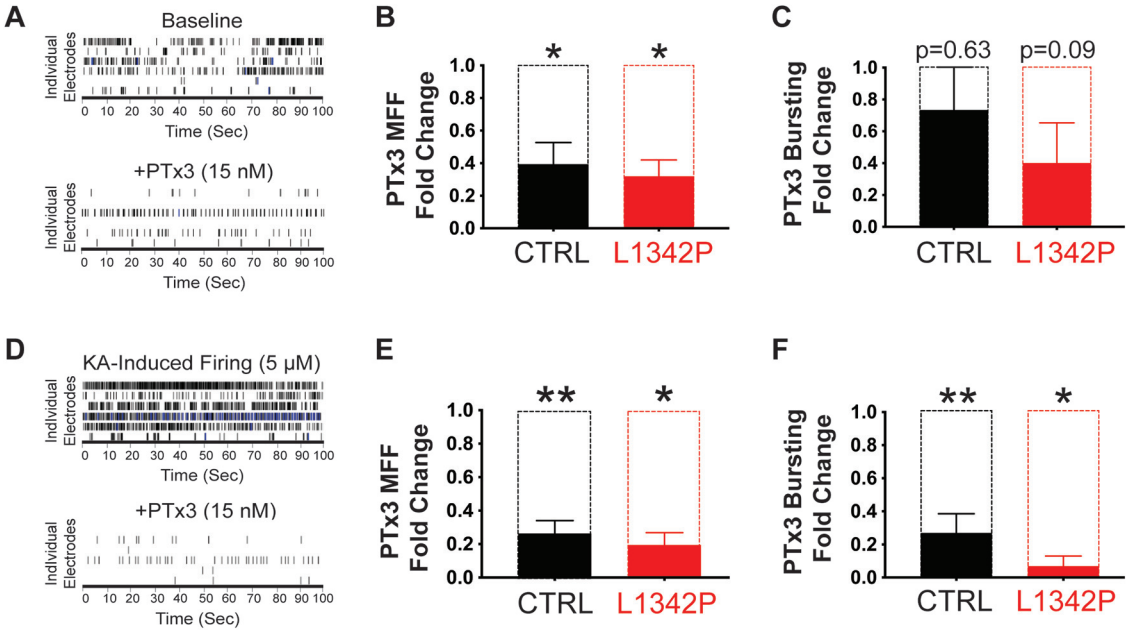

Figure 7. PTx3 effectively suppresses spontaneous and KA-induced firings of hiPSC-derived neurons carrying the L1342P variant. ***A***, MEA recordings showed that baseline mean firing frequency (MFF) was reduced after the addition of PTx3 in L1342P culture. ***B***, PTx3 significantly inhibited the baseline firing in both isogenic control and L1342P culture. ***C***, PTx3 did not significantly reduce the bursting frequency in either isogenic control or L1342P cultures. In ***B***, ***C***, Wilcoxon test was performed to compare the neuronal firing before and after the PTx3 treatment; $*p < 0.05$. ***D***, KA enhanced neuronal firing by elevating the bursting, which can be effectively inhibited by PTx3. ***E***, PTx3 significantly inhibited the MFF in both control and L1342P neuron culture after KA-mediated stimulation. ***F***, PTx3 significantly inhibited the bursting frequency in both control and L13432P neuron culture after KA-mediated stimulation. In ***E***, ***F***, Wilcoxon test was performed to compare the KA-treated cultures before and after the PTx3 treatment. Mann–Whitney *U* test was performed to compare the PTx3 effects between control and L1342P culture. In the experiment of testing PTx3 effect on baseline firing, the sample size was $n = 6$ wells for control cultures and $n = 6$ wells for L1342P cultures. In the experiment of testing PTx3 effect on KA-induced firing, the sample size was $n = 8$ wells for control cultures and $n = 6$ wells for L1342P cultures; $*p < 0.05$, $**p < 0.01$.

that the Nav1.2 current is one of the components contributing to the total sodium current in these neurons, consistent with the literature (Ye et al., 2018).

We used MEA recordings to test the inhibitory effect of PTx3 on baseline neuronal firings. After adding PTx3, the neuronal firing from L1342P cultures was reduced markedly (Fig. 7*A*). Quantitatively, a highly effective and significant reduction of baseline firing was observed in both isogenic control and L1342P cultures (control: 0.39 ± 0.10, relative to baseline, $n = 6$, $p = 0.03$; L1342P: 0.32 ± 0.01, relative to baseline, $n = 6$, $p = 0.03$, Wilcoxon test; Fig. 7*B*). No significant difference in fold change was found between control and L1342P groups ($p = 0.86$, Mann–Whitney *U* test). However, we did not observe a significant reduction in bursting frequency for either culture (control: 0.73 ± 0.28, relative to baseline, $n = 5$, $p = 0.63$; L1342P: 0.40 ± 0.25, relative to baseline, $n = 6$, $p = 0.09$, Wilcoxon test; Fig. 7*C*). No significant difference in fold change was found between control and L1342P groups ($p = 0.45$, Mann–Whitney *U* test). For synchrony index measurement, we found a significant reduction in L1342P cultures, but not in the control group (control: 0.65 ± 0.26, relative to baseline, $n = 6$, $p = 0.22$; L1342P: 0.36 ± 0.12, relative to baseline, $n = 6$, $p = 0.03$, Wilcoxon test). No significant difference in fold change was found between control and L1342P groups ($p = 0.48$, Mann–Whitney *U* test). Additionally, we evaluated the potency of PTx3 to inhibit neuronal firings under the condition of chemically-induced hyperexcitability to further model seizure states. KA (5 μM), a glutamate receptor agonist and a commonly used compound to chemically trigger epileptiform activities, was added to isogenic control and L1342P cultures (Odawara et al., 2016; Taga et al., 2019). We found that KA was able to markedly enhance the firings of both cultures (KA-induced MFF fold change: control: 2.28 ± 0.46, $n = 8$; L1342P: 2.04 ± 0.32, $n = 6$, $p = 0.99$, Mann–Whitney *U* test; Fig. 7*D*, upper panel). With the addition of PTx3, we observed a strong reduction in the spike numbers (Fig. 7*D*, lower panel). Both MFF and bursting frequency were significantly reduced by PTx3 in both isogenic control and L1342P neuronal culture (Fig. 7*E*,*F*), while no significant decrease was observed in the synchrony index (MFF: control: 0.26 ± 0.07, relative to KA-induced activity, $n = 8$, $p = 0.007$; L1342P: 0.20 ± 0.07, relative to KA-induced activity, $n = 6$, $p = 0.03$. Bursting frequency: control: 0.27 ± 0.1, relative to KA-induced activity, $n = 8$, $p = 0.007$; L1342P: 0.07 ± 0.06, relative to KA-induced activity, $n = 6$, $p = 0.03$. Synchrony index: control: 0.69 ± 0.20, relative to KA-induced activity, $n = 8$, $p = 0.14$; L1342P: 0.32 ± 0.12, relative to KA-induced activity, $n = 4$, $p = 0.13$, Wilcoxon test). No significant difference in fold change was found between control and L1342P groups (Mann–Whitney *U* test). Interestingly, PTx3 seems to have a slightly stronger inhibitory effect on L1342P cultures compared with isogenic control cultures (Fig. 7*B*,*C*,*E*,*F*). Our results show that the PTx3 could effectively alleviate the hyperexcitability of neuronal culture with the L1342P variant, supporting the hypothesis that isoform-specific Nav1.2 blockers could potentially be novel anticonvulsant drugs.

Discussion

In this study, we revealed substantial and complex biophysical property changes in the L1342P variant of the Nav1.2 sodium channel, which manifested as hyperexcitability of cortical neurons. In particular, we found that cortical neurons derived from hiPSCs carrying heterozygous L1342P display significantly enhanced sustainable AP firings, larger spike amplitude, hyperpolarized voltage threshold, lower rheobase, and greater sodium current density with substantial shift in channel activation. By

investigating the network activity of neuronal populations using MEA recordings, we revealed increased network excitability with burst firing and a higher synchrony index in the L1342P culture. Remarkably, we obtained evidence to show that hiPSC-derived neurons carrying the L1342P variant are less sensitive to a commonly used anticonvulsant compound phenytoin but have equal or slightly stronger sensitivity to a Nav1.2 isoform-specific blocker.

Nav1.1, Nav1.2, and Nav1.6 are three major voltage-gated sodium channels expressed in the CNS (Trimmer and Rhodes, 2004). Notably, variants in all these channels are associated with seizures, probably because of their important roles in mediating AP firing (Musto et al., 2020; Meisler et al., 2021). Among them, Nav1.1 is strongly expressed in interneurons (Ogiwara et al., 2007). The majority of the seizure-associated Nav1.1 variants are suggested to display loss-of-function phenotype, which reduces the excitability of inhibitory interneurons, leading to less inhibition on principal excitatory neurons (Catterall et al., 2010). In turn, without sufficient inhibition, excitatory neurons become more excitable and promote seizures. On the other hand, both Nav1.2 and Nav1.6 are predominantly expressed in principal excitatory neurons (Ye et al., 2018). Epilepsy-associated Nav1.6 variants are mainly gain-of-function. Studies found that enhanced excitability of hiPSC-derived excitatory neurons is the primary mechanism underlying the gain-of-function Nav1.6 variant-related seizures (Tidball et al., 2020). Loss-of-function variants of Nav1.6 are also found in some patients, but these patients generally do not develop epileptic phenotypes (Gardella and Møller, 2019). In contrast, the association between variants in Nav1.2 and seizure is more complicated (Kamiya et al., 2004; Howell et al., 2015; Hedrich et al., 2019; Reynolds et al., 2020; Eaton et al., 2021b). Intriguingly, seizures have been found to be associated with both gain-of-function and loss-of-function Nav1.2 variants (Wolff et al., 2017, 2019; Kaczmarek, 2021; Spratt et al., 2021; Zhang et al., 2021). Since Nav1.2 is expressed in principal excitatory neurons, it is predicted that Nav1.2 variants would enhance neuronal excitability. Nevertheless, this hypothesis has not been explicitly tested in human neurons. Here, we showed, for the first time, that the epilepsy-associated Nav1.2 variant L1342P causes hyperexcitability and hypersynchronous firing in human excitatory neurons derived from hiPSCs. Mechanistically, we revealed that the L1342P variant resulted in a hyperpolarized activation shift with enhanced sodium current density. We proposed a working hypothesis that the extra Nav1.2 channels available in the cell membrane, which possess altered biophysical properties to be more readily activated, are likely to push neurons into a hyperexcitable state to promote seizures.

Interestingly, despite an overall gain-of-function phenotype associated with neuronal hyperexcitability, we also observed loss-of-function traits, particularly in AP firing. In the input-output relationship, we found that the L1342P neurons initially had a strong response to the current stimulus by increasing AP firing significantly. However, the L1342P neurons later failed to maintain sustainability in firing frequency at high current injection (Fig. 5*B*). A similar trend of the input-output relationship was reported in a previously described variant Q1478K in Nav1.1 (Cestèle et al., 2008). The Q1478K variant caused a "self-limiting" hyperexcitability phenotype, possibly caused by a significant reduction in sodium current density (Cestèle et al., 2008). However, we found an increased current density in L1342P, suggesting a different mechanism. We propose that the failure to maintain spiking could result from enhanced inactivation of the Nav1.2-L1342P mutant channel, which was discovered in our biophysical assays. Further studies are required to test this possible mechanism.

Several recently reported variants in *SCN2A* from patients with childhood epilepsy also presented with evidence indicating developmental impairments (Miao et al., 2020). The terminology of "developmental and/or epileptic encephalopathy" thus has been used to imply that the developmental impairments could occur independently of seizures (Maljevic et al., 2017; Scheffer et al., 2017). Indeed, profiling patients with the L1342P variant revealed developmental disorders (Hackenberg et al., 2014; Matalon et al., 2014; Dimassi et al., 2016). Three out of five L1342P cases display microcephaly, brain volume loss, and reduced head circumference. It is currently unknown whether the developmental impairments observed in patients carrying L1342P are related to or independent of the seizures caused by the L1342P variant. These disease symptoms related to neurodevelopment require careful investigation in the future.

Studies have traditionally used heterologous expression system as a convenient platform to study ion channel variants related to epilepsies. This type of analysis is informative regarding the specific biophysical properties of a particular variant (Ben-Shalom et al., 2017; Berecki et al., 2018; Mason et al., 2019). Moreover, biophysical analysis can also provide information regarding the "gain-of-function" versus the "loss-of-function" feature of a particular variant of interest (Adney et al., 2020; Thompson et al., 2020). Determining a gain versus loss-of-function is critically important, both for establishing genotype-phenotype correlations and informing clinical practice. Indeed, an insightful clinical study has shown that seizures patients carrying traditional "gain-of-function" Nav1.2 variants can be adequately controlled by sodium channel blockers, whereas this same class of sodium channel blockers exacerbate seizures and worsen outcomes for patients carrying loss-of-function Nav1.2 variants (Wolff et al., 2017, 2019). Using electrophysiology and human neurons derived from hiPSCs, here we provided evidence to show that neuron carrying Nav1.2-L1342P variant have a gain-of-function phenotype, despite complex biophysical properties revealed in the heterologous expression system.

Even with advanced genetic testing, controlling seizures is still challenging in clinical practice. The standard AED guidelines are usually applied to patients indiscriminately (Wilmshurst et al., 2015; Sanders et al., 2018). Many patients do not respond to the first AED prescribed to them, and they have to go through a trial-and-error process with different medications. This tedious and often ineffective process significantly increases disease burden and may cause the optimal treatment window to be missed for children with epilepsy. Therefore, there is an urgent need to explore new approaches to guide clinical practice in a precision medicine manner. hiPSC-based *in vitro* genetic models hold great promise to transform clinical practice. Neurons derived from hiPSCs are amenable for high-throughput parallel screening for targeted drug discovery. Pairing with MEA, a high-throughput, extracellular recording assay of neuronal activity (Odawara et al., 2016, 2018; Tukker et al., 2020a; Verma et al., 2020), such studies have been attempted. Using hiPSC-derived neurons, it was recently found that riluzole and phenytoin can target specific Nav1.6 variants to attenuate bursting phenotypes *in vitro* (Tidball et al., 2020). Notably, effective compounds identified in hiPSC models successfully suppress seizure events of patients in the clinical study, highlighting the translational value of the *in vitro* hiPSC-based platform (Tidball et al., 2020). PTx3, one of the experimental Nav1.2 blockers, was studied previously

for its specificity against several sodium channel subtypes. PTx3 is one of the most potent Nav1.2 blockers, with an IC_{50} value of 0.6 ± 0.1 nM in the heterologous expression system (Bosmans et al., 2006). It blocks Nav1.6 at around 100 nM and can also block Nav1.1 with an IC_{50} values of ~610 nM (Bosmans et al., 2006). In the study of mammalian neurons, a dose below 30 nM was often used, and its specificity was retained (Li et al., 2014; Yin et al., 2017; Davis et al., 2020; Risner et al., 2020). In our study, we used 15 nM of PTx3, a concentration in the range that can achieve high Nav1.2 specificity. We found that PTx3 can effectively reduce the enhanced firing of neurons carrying the Nav1.2-L1342P variant, suggesting that the development of novel Nav1.2 specific blocker may benefit patients affected by gain-of-function Nav1.2 variants.

While using a patient-derived hiPSC line could directly model subject-specific phenotypes and interindividual differences (Mis et al., 2019), the use of reference hiPSCs with genetic variants engineered by CRISPR/Cas9 is a useful complementary approach. This approach takes advantage of a standardized genetic background of reference iPSCs line as the "baseline" for cross-variant comparisons, and provides a reproducible control for potential drug discovery efforts targeting recurring genetic variants. Indeed, this approach has been used in a large-scale project to introduce disease-associated variants into reference hiPSCs to model neurodegenerative disorders (Ramos et al., 2021). In this study, we showed that reference hiPSC-derived neurons carrying the drug-resistant Nav1.2-L1342P variant were not sensitive to phenytoin but had equal or even stronger sensitivity toward an experimental isoform-specific Nav1.2 blocker. Our results demonstrated the usefulness of such an *in vitro* platform to potentially advance drug selection and discovery, which warrants additional studies to streamline this process for future clinical translation.

In summary, we reveal a hyperexcitability phenotype in hiPSC-derived neurons carrying the Nav1.2-L1342P variant, with unique features as possible pathogenic mechanisms. Moreover, we demonstrate that our *in vitro* model is able to partially recapitulate the pharmaco-responsiveness of the Nav1.2-L1342P variant. Using this *in vitro* model, we further show, as a proof-of-principle, that an isoform-specific Nav1.2 blocker may be an effective treatment for hyperexcitability caused by Nav1.2 gain-of-function variants. Our results highlight the utility of genome-edited, hiPSC-derived neurons for mechanistic investigations of disease-causing variants, as well as for drug discovery to advance personalized treatment for patients carrying a variety of genetic variants.

References

Adney SK, Millichap JJ, DeKeyser JM, Abramova T, Thompson CH, George AL Jr (2020) Functional and pharmacological evaluation of a novel SCN2A variant linked to early-onset epilepsy. Ann Clin Transl Neurol 7:1488–1501.

Begemann A, Acuña MA, Zweier M, Vincent M, Steindl K, Bachmann-Gagescu R, Hackenberg A, Abela L, Plecko B, Kroell-Seger J, Baumer A, Yamakawa K, Inoue Y, Asadollahi R, Sticht H, Zeilhofer HU, Rauch A (2019) Further corroboration of distinct functional features in SCN2A variants causing intellectual disability or epileptic phenotypes. Mol Med 25:6.

Ben-Shalom R, Keeshen CM, Berrios KN, An JY, Sanders SJ, Bender KJ (2017) Opposing effects on NaV1.2 function underlie differences between SCN2A variants observed in individuals with autism spectrum disorder or infantile seizures. Biol Psychiatry 82:224–232.

Berecki G, Howell KB, Deerasooriya YH, Cilio MR, Oliva MK, Kaplan D, Scheffer IE, Berkovic SF, Petrou S (2018) Dynamic action potential clamp predicts functional separation in mild familial and severe de novo forms of SCN2A epilepsy. Proc Natl Acad Sci USA 115:E5516–E5525.

Bialer M, Johannessen SI, Koepp MJ, Levy RH, Perucca E, Tomson T, White HS (2018) Progress report on new antiepileptic drugs: a summary of the Fourteenth Eilat Conference on New Antiepileptic Drugs and Devices (EILAT XIV). I. Drugs in preclinical and early clinical development. Epilepsia 59:1811–1841.

Boerma RS, Braun KP, van den Broek MPH, van de Broek MPH, van Berkestijn FMC, Swinkels ME, Hagebeuk EO, Lindhout D, van Kempen M, Boon M, Nicolai J, de Kovel CG, Brilstra EH, Koeleman BPC (2016) Remarkable phenytoin sensitivity in 4 children with SCN8A-related epilepsy: a molecular neuropharmacological approach. Neurotherapeutics 13:192–197.

Boissart C, Poulet A, Georges P, Darville H, Julita E, Delorme R, Bourgeron T, Peschanski M, Benchoua A (2013) Differentiation from human pluripotent stem cells of cortical neurons of the superficial layers amenable to psychiatric disease modeling and high-throughput drug screening. Transl Psychiatry 3:e294.

Bosmans F, Rash L, Zhu S, Diochot S, Lazdunski M, Escoubas P, Tytgat J (2006) Four novel tarantula toxins as selective modulators of voltage-gated sodium channel subtypes. Mol Pharmacol 69:419–429.

Braakman HM, Verhoeven JS, Erasmus CE, Haaxma CA, Willemsen MH, Schelhaas HJ (2017) Phenytoin as a last-resort treatment in SCN8A encephalopathy. Epilepsia Open 2:343–344.

Catterall WA, Kalume F, Oakley JC (2010) NaV1.1 channels and epilepsy. J Physiol 588:1849–1859.

Cestèle S, Scalmani P, Rusconi R, Terragni B, Franceschetti S, Mantegazza M (2008) Self-limited hyperexcitability: functional effect of a familial hemiplegic migraine mutation of the Nav1.1 (SCN1A) Na+ channel. J Neurosci 28:7273–7283.

Davis H, Herring N, Paterson DJ (2020) Downregulation of M current is coupled to membrane excitability in sympathetic neurons before the onset of hypertension. Hypertension 76:1915–1923.

Deneault E, Faheem M, White SH, Rodrigues DC, Sun S, Wei W, Piekna A, Thompson T, Howe JL, Chalil L, Kwan V, Walker S, Pasceri P, Roth FP, Yuen RK, Singh KK, Ellis J, Scherer SW (2019) CNTN5(-)(/+)or EHMT2(-)(/+)human iPSC-derived neurons from individuals with autism develop hyperactive neuronal networks. Elife 8:e40092.

Dimassi S, Labalme A, Ville D, Calender A, Mignot C, Boutry-Kryza N, de Bellescize J, Rivier-Ringenbach C, Bourel-Ponchel E, Cheillan D, Simonet T, Maincent K, Rossi M, Till M, Mougou-Zerelli S, Edery P, Saad A, Heron D, des Portes V, Sanlaville D, et al. (2016) Whole-exome sequencing improves the diagnosis yield in sporadic infantile spasm syndrome. Clin Genet 89:198–204.

Eaton M, Que Z, Zhang J, Beck K, Shi R, McDermott J, Ladisch M, Yang Y (2021a) Multi-electrode array of sensory neurons as an in vitro platform to identify the nociceptive response to pharmaceutical buffer systems of injectable biologics. Pharm Res 38:1179–1186.

Eaton M, Zhang J, Ma Z, Park AC, Lietzke E, Romero CM, Liu Y, Coleman ER, Chen X, Xiao T, Que Z, Lai S, Wu J, Lee JH, Palant S, Nguyen HP, Huang Z, Skarnes WC, Koss WA, Yang Y (2021b) Generation and basic characterization of a gene-trap knockout mouse model of Scn2a with a substantial reduction of voltage-gated sodium channel Nav 1.2 expression. Genes Brain Behav 20:e12725.

Eggermont JJ (2006) Properties of correlated neural activity clusters in cat auditory cortex resemble those of neural assemblies. J Neurophysiol 96:746–764.

Fruscione F, Valente P, Sterlini B, Romei A, Baldassari S, Fadda M, Prestigio C, Giansante G, Sartorelli J, Rossi P, Rubio A, Gambardella A, Nieus T, Broccoli V, Fassio A, Baldelli P, Corradi A, Zara F, Benfenati F (2018) PRRT2 controls neuronal excitability by negatively modulating Na+ channel 1.2/1.6 activity. Brain 141:1000–1016.

Gardella E, Møller RS (2019) Phenotypic and genetic spectrum of SCN8A-related disorders, treatment options, and outcomes. Epilepsia 60 [Suppl 3]:S77–S85.

Gardella E, Marini C, Trivisano M, Fitzgerald MP, Alber M, Howell KB, Darra F, Siliquini S, Bölsterli BK, Masnada S, Pichiecchio A, Johannesen KM, Jepsen B, Fontana E, Anibaldi G, Russo S, Cogliati F, Montomoli M, Specchio N, et al. (2018) The phenotype of SCN8A developmental and epileptic encephalopathy. Neurology 91:e1112–e1124.

Ghatak S, Dolatabadi N, Trudler D, Zhang X, Wu Y, Mohata M, Ambasudhan R, Talantova M, Lipton SA (2019) Mechanisms of hyperexcitability in Alzheimer's disease hiPSC-derived neurons and cerebral organoids vs isogenic controls. Elife 8:e50333.

Gorman KM, King MD (2017) SCN2A p.Ala263Val variant a phenotype of neonatal seizures followed by paroxysmal ataxia in toddlers. Pediatr Neurol 67:111–112.

Hackenberg A, Baumer A, Sticht H, Schmitt B, Kroell-Seger J, Wille D, Joset P, Papuc S, Rauch A, Plecko B (2014) Infantile epileptic encephalopathy, transient choreoathetotic movements, and hypersomnia due to a De Novo missense mutation in the SCN2A gene. Neuropediatrics 45:261–264.

Hallermann S, de Kock CP, Stuart GJ, Kole MH (2012) State and location dependence of action potential metabolic cost in cortical pyramidal neurons. Nat Neurosci 15:1007–1014.

Halliwell RF, Salmanzadeh H, Coyne L, Cao WS (2021) An electrophysiological and pharmacological study of the properties of human iPSC-derived neurons for drug discovery. Cells 10:1953.

Hedrich UBS, Lauxmann S, Lerche H (2019) SCN2A channelopathies: mechanisms and models. Epilepsia 60 [Suppl 3]:S68–S76.

Howell KB, McMahon JM, Carvill GL, Tambunan D, Mackay MT, Rodriguez-Casero V, Webster R, Clark D, Freeman JL, Calvert S, Olson HE, Mandelstam S, Poduri A, Mefford HC, Harvey AS, Scheffer IE (2015) SCN2A encephalopathy: a major cause of epilepsy of infancy with migrating focal seizures. Neurology 85:958–966.

Hu W, Tian C, Li T, Yang M, Hou H, Shu Y (2009) Distinct contributions of Na(v)1.6 and Na(v)1.2 in action potential initiation and backpropagation. Nat Neurosci 12:996–1002.

Jiruska P, de Curtis M, Jefferys JG, Schevon CA, Schiff SJ, Schindler K (2013) Synchronization and desynchronization in epilepsy: controversies and hypotheses. J Physiol 591:787–797.

Kaczmarek LK (2021) The NaVy paradox: reducing sodium currents increases excitability. Trends Neurosci 44:767–768.

Kamiya K, Kaneda M, Sugawara T, Mazaki E, Okamura N, Montal M, Makita N, Tanaka M, Fukushima K, Fujiwara T, Inoue Y, Yamakawa K (2004) A nonsense mutation of the sodium channel gene SCN2A in a patient with intractable epilepsy and mental decline. J Neurosci 24:2690–2698.

Kilpinen H, Goncalves A, Leha A, Afzal V, Alasoo K, Ashford S, Bala S, Bensaddek D, Casale FP, Culley OJ, Danecek P, Faulconbridge A, Harrison PW, Kathuria A, McCarthy D, McCarthy SA, Meleckyte R, Memari Y, Moens N, Soares F, et al. (2017) Common genetic variation drives molecular heterogeneity in human iPSCs. Nature 546:370–375.

Kouroupi G, Taoufik E, Vlachos IS, Tsioras K, Antoniou N, Papastefanaki F, Chroni-Tzartou D, Wrasidlo W, Bohl D, Stellas D, Politis PK, Vekrellis K, Papadimitriou D, Stefanis L, Bregestovski P, Hatzigeorgiou AG, Masliah E, Matsas R (2017) Defective synaptic connectivity and axonal neuropathology in a human iPSC-based model of familial Parkinson's disease. Proc Natl Acad Sci USA 114:E3679–E3688.

Li J, Cai T, Jiang Y, Chen H, He X, Chen C, Li X, Shao Q, Ran X, Li Z, Xia K, Liu C, Sun ZS, Wu J (2016) Genes with de novo mutations are shared by four neuropsychiatric disorders discovered from NPdenovo database. Mol Psychiatry 21:298.

Li T, Tian C, Scalmani P, Frassoni C, Mantegazza M, Wang Y, Yang M, Wu S, Shu Y (2014) Action potential initiation in neocortical inhibitory interneurons. PLoS Biol 12:e1001944.

Liao Y, Deprez L, Maljevic S, Pitsch J, Claes L, Hristova D, Jordanova A, Ala-Mello S, Bellan-Koch A, Blazevic D, Schubert S, Thomas EA, Petrou S, Becker AJ, De Jonghe P, Lerche H (2010) Molecular correlates of age-dependent seizures in an inherited neonatal-infantile epilepsy. Brain 133:1403–1414.

Liu Y, Lopez-Santiago LF, Yuan Y, Jones JM, Zhang H, O'Malley HA, Patino GA, O'Brien JE, Rusconi R, Gupta A, Thompson RC, Natowicz MR, Meisler MH, Isom LL, Parent JM (2013) Dravet syndrome patient-derived neurons suggest a novel epilepsy mechanism. Ann Neurol 74:128–139.

Lu C, Shi X, Allen A, Baez-Nieto D, Nikish A, Sanjana NE, Pan JQ (2019) Overexpression of NEUROG2 and NEUROG1 in human embryonic stem cells produces a network of excitatory and inhibitory neurons. FASEB J 33:5287–5299.

Maljevic S, Reid CA, Petrou S (2017) Models for discovery of targeted therapy in genetic epileptic encephalopathies. J Neurochem 143:30–48.

Mason ER, Wu F, Patel RR, Xiao Y, Cannon SC, Cummins TR (2019) Resurgent and gating pore currents induced by de novo SCN2A epilepsy mutations. eNeuro 6:ENEURO.0141-19.2019.

Matalon D, Goldberg E, Medne L, Marsh ED (2014) Confirming an expanded spectrum of SCN2A mutations: a case series. Epileptic Disord 16:13–18.

Mehta SR, Tom CM, Wang Y, Bresee C, Rushton D, Mathkar PP, Tang J, Mattis VB (2018) Human Huntington's disease iPSC-derived cortical neurons display altered transcriptomics, morphology, and maturation. Cell Rep 25:1081–1096.e6.

Meisler MH, Hill SF, Yu W (2021) Sodium channelopathies in neurodevelopmental disorders. Nat Rev Neurosci 22:152–166.

Miao P, Tang S, Ye J, Wang J, Lou Y, Zhang B, Xu X, Chen X, Li Y, Feng J (2020) Electrophysiological features: the next precise step for SCN2A developmental epileptic encephalopathy. Mol Genet Genomic Med 8: e1250.

Mis MA, Yang Y, Tanaka BS, Gomis-Perez C, Liu S, Dib-Hajj F, Adi T, Garcia-Milian R, Schulman BR, Dib-Hajj SD, Waxman SG (2019) Resilience to pain: a peripheral component identified using induced pluripotent stem cells and dynamic clamp. J Neurosci 39:382–392.

Misra SN, Kahlig KM, George AL Jr (2008) Impaired NaV1.2 function and reduced cell surface expression in benign familial neonatal-infantile seizures. Epilepsia 49:1535–1545.

Musto E, Gardella E, Møller RS (2020) Recent advances in treatment of epilepsy-related sodium channelopathies. Eur J Paediatr Neurol 24:123–128.

Odawara A, Katoh H, Matsuda N, Suzuki I (2016) Physiological maturation and drug responses of human induced pluripotent stem cell-derived cortical neuronal networks in long-term culture. Sci Rep 6:26181.

Odawara A, Matsuda N, Ishibashi Y, Yokoi R, Suzuki I (2018) Toxicological evaluation of convulsant and anticonvulsant drugs in human induced pluripotent stem cell-derived cortical neuronal networks using an MEA system. Sci Rep 8:10416.

Ogiwara I, Miyamoto H, Morita N, Atapour N, Mazaki E, Inoue I, Takeuchi T, Itohara S, Yanagawa Y, Obata K, Furuichi T, Hensch TK, Yamakawa K (2007) Nav1.1 localizes to axons of parvalbumin-positive inhibitory interneurons: a circuit basis for epileptic seizures in mice carrying an Scn1a gene mutation. J Neurosci 27:5903–5914.

Pan X, Li Z, Huang X, Huang G, Gao S, Shen H, Liu L, Lei J, Yan N (2019) Molecular basis for pore blockade of human Na(+) channel $Na_v1.2$ by the μ-conotoxin KIIIA. Science 363:1309–1313.

Parker SS, Moutal A, Cai S, Chandrasekaran S, Roman MR, Koshy AA, Khanna R, Zinsmaier KE, Mouneimne G (2018) High fidelity cryopreservation and recovery of primary rodent cortical neurons. eNeuro 5: ENEURO.0135-18.2018.

Patlak J (1991) Molecular kinetics of voltage-dependent Na+ channels. Physiol Rev 71:1047–1080.

Quraishi IH, Stern S, Mangan KP, Zhang Y, Ali SR, Mercier MR, Marchetto MC, McLachlan MJ, Jones EM, Gage FH, Kaczmarek LK (2019) An epilepsy-associated KCNT1 mutation enhances excitability of human iPSC-derived neurons by increasing slack KNa currents. J Neurosci 39:7438–7449.

Ramos DM, Skarnes WC, Singleton AB, Cookson MR, Ward ME (2021) Tackling neurodegenerative diseases with genomic engineering: a new stem cell initiative from the NIH. Neuron 109:1080–1083.

Reynolds C, King MD, Gorman KM (2020) The phenotypic spectrum of SCN2A-related epilepsy. Eur J Paediatr Neurol 24:117–122.

Risner ML, McGrady NR, Pasini S, Lambert WS, Calkins DJ (2020) Elevated ocular pressure reduces voltage-gated sodium channel NaV1.2 protein expression in retinal ganglion cell axons. Exp Eye Res 190:107873.

Rusconi R, Scalmani P, Cassulini RR, Giunti G, Gambardella A, Franceschetti S, Annesi G, Wanke E, Mantegazza M (2007) Modulatory proteins can rescue a trafficking defective epileptogenic Na(v)1.1 Na+ channel mutant. J Neurosci 27:11037–11046.

Rush AM, Dib-Hajj SD, Waxman SG (2005) Electrophysiological properties of two axonal sodium channels, Nav1.2 and Nav1.6, expressed in mouse spinal sensory neurones. J Physiol 564:803–815.

Sanders SJ, Campbell AJ, Cottrell JR, Moller RS, Wagner FF, Auldridge AL, Bernier RA, Catterall WA, Chung WK, Empfield JR, George AL, Hipp JF, Khwaja O, Kiskinis E, Lal D, Malhotra D, Millichap JJ, Otis TS, Petrou S, Pitt G, et al. (2018) Progress in understanding and treating SCN2A-mediated disorders. Trends Neurosci 41:442–456.

Satir TM, Nazir FH, Vizlin-Hodzic D, Hardselius E, Blennow K, Wray S, Zetterberg H, Agholme L, Bergström P (2020) Accelerated neuronal and synaptic maturation by BrainPhys medium increases Abeta secretion and

alters Abeta peptide ratios from iPSC-derived cortical neurons. Sci Rep 10:601.

Scheffer IE, Berkovic S, Capovilla G, Connolly MB, French J, Guilhoto L, Hirsch E, Jain S, Mathern GW, Moshé SL, Nordli DR, Perucca E, Tomson T, Wiebe S, Zhang YH, Zuberi SM (2017) ILAE classification of the epilepsies: position paper of the ILAE commission for classification and terminology. Epilepsia 58:512–521.

Schmidt-Hieber C, Bischofberger J (2010) Fast sodium channel gating supports localized and efficient axonal action potential initiation. J Neurosci 30:10233–10242.

Shi Y, Kirwan P, Livesey FJ (2012a) Directed differentiation of human pluripotent stem cells to cerebral cortex neurons and neural networks. Nat Protoc 7:1836–1846.

Shi Y, Kirwan P, Smith J, Robinson HP, Livesey FJ (2012b) Human cerebral cortex development from pluripotent stem cells to functional excitatory synapses. Nat Neurosci 15:477–486, S1.

Shorvon SD (2011) The etiologic classification of epilepsy. Epilepsia 52:1052–1057.

Siddiqi FH, Menzies FM, Lopez A, Stamatakou E, Karabiyik C, Ureshino R, Ricketts T, Jimenez-Sanchez M, Esteban MA, Lai L, Tortorella MD, Luo Z, Liu H, Metzakopian E, Fernandes HJR, Bassett A, Karran E, Miller BL, Fleming A, Rubinsztein DC (2019) Felodipine induces autophagy in mouse brains with pharmacokinetics amenable to repurposing. Nat Commun 10:1817.

Skarnes WC, Pellegrino E, McDonough JA (2019) Improving homology-directed repair efficiency in human stem cells. Methods 164-165:18–28.

Spratt PWE, Ben-Shalom R, Keeshen CM, Burke KJ Jr, Clarkson RL, Sanders SJ, Bender KJ (2019) The autism-associated gene Scn2a contributes to dendritic excitability and synaptic function in the prefrontal cortex. Neuron 103:673–685.e5.

Spratt PWE, Alexander RPD, Ben-Shalom R, Sahagun A, Kyoung H, Keeshen CM, Sanders SJ, Bender KJ (2021) Paradoxical hyperexcitability from NaV1.2 sodium channel loss in neocortical pyramidal cells. Cell Rep 36:109483.

Streeter I, Harrison PW, Faulconbridge A, Flicek P, Parkinson H, Clarke L; The HipSci Consortium (2017) The human-induced pluripotent stem cell initiative-data resources for cellular genetics. Nucleic acids Res 45: D691–D697.

Syrbe S, Zhorov BS, Bertsche A, Bernhard MK, Hornemann F, Mütze U, Hoffmann J, Hörtnagel K, Kiess W, Hirsch FW, Lemke JR, Merkenschlager A (2016) Phenotypic variability from benign infantile epilepsy to Ohtahara syndrome associated with a novel mutation in SCN2A. Mol Syndromol 7:182–188.

Taga A, Dastgheyb R, Habela C, Joseph J, Richard JP, Gross SK, Lauria G, Lee G, Haughey N, Maragakis NJ (2019) Role of human-induced pluripotent stem cell-derived spinal cord astrocytes in the functional maturation of motor neurons in a multielectrode array system. Stem Cells Transl Med 8:1272–1285.

Thompson CH, Ben-Shalom R, Bender KJ, George AL (2020) Alternative splicing potentiates dysfunction of early-onset epileptic encephalopathy SCN2A variants. J Gen Physiol 152:e201912442.

Tian C, Wang K, Ke W, Guo H, Shu Y (2014) Molecular identity of axonal sodium channels in human cortical pyramidal cells. Front Cell Neurosci 8:297.

Tidball AM, Lopez-Santiago LF, Yuan Y, Glenn TW, Margolis JL, Clayton Walker J, Kilbane EG, Miller CA, Martina Bebin E, Scott Perry M, Isom LL, Parent JM (2020) Variant-specific changes in persistent or resurgent sodium current in SCN8A-related epilepsy patient-derived neurons. Brain 143:3025–3040.

Trimmer JS, Rhodes KJ (2004) Localization of voltage-gated ion channels in mammalian brain. Annu Rev Physiol 66:477–519.

Tukker AM, Wijnolts FMJ, de Groot A, Westerink RHS (2018) Human iPSC-derived neuronal models for in vitro neurotoxicity assessment. Neurotoxicology 67:215–225.

Tukker AM, Wijnolts FMJ, de Groot A, Westerink RHS (2020a) Applicability of hiPSC-derived neuronal cocultures and rodent primary cortical cultures for in vitro seizure liability assessment. Toxicol Sci 178:71–87.

Tukker AM, Van Kleef R, Wijnolts FMJ, De Groot A, Westerink RHS (2020b) Towards animal-free neurotoxicity screening: applicability of hiPSC-derived neuronal models for in vitro seizure liability assessment. ALTEX 37:121–135.

Verma P, Eaton M, Kienle A, Flockerzi D, Yang Y, Ramkrishna D (2020) Examining sodium and potassium channel conductances involved in hyperexcitability of chemotherapy-induced peripheral neuropathy: a mathematical and cell culture-based study. Front Comput Neurosci 14:564980.

Wilmshurst JM, Gaillard WD, Vinayan KP, Tsuchida TN, Plouin P, Van Bogaert P, Carrizosa J, Elia M, Craiu D, Jovic NJ, Nordli D, Hirtz D, Wong V, Glauser T, Mizrahi EM, Cross JH (2015) Summary of recommendations for the management of infantile seizures: task Force Report for the ILAE Commission of Pediatrics. Epilepsia 56:1185–1197.

Wolff M, Johannesen KM, Hedrich UBS, Masnada S, Rubboli G, Gardella E, Lesca G, Ville D, Milh M, Villard L, Afenjar A, Chantot-Bastaraud S, Mignot C, Lardennois C, Nava C, Schwarz N, Gérard M, Perrin L, Doummar D, Auvin S, et al. (2017) Genetic and phenotypic heterogeneity suggest therapeutic implications in SCN2A-related disorders. Brain 140:1316–1336.

Wolff M, Brunklaus A, Zuberi SM (2019) Phenotypic spectrum and genetics of SCN2A-related disorders, treatment options, and outcomes in epilepsy and beyond. Epilepsia 60 [Suppl 3]:S59–S67.

Yang Y, Huang J, Mis MA, Estacion M, Macala L, Shah P, Schulman BR, Horton DB, Dib-Hajj SD, Waxman SG (2016) Nav1.7-A1632G mutation from a family with inherited erythromelalgia: enhanced firing of dorsal root ganglia neurons evoked by thermal stimuli. J Neurosci 36:7511–7522.

Yang Y, Adi T, Effraim PR, Chen L, Dib-Hajj SD, Waxman SG (2018) Reverse pharmacogenomics: carbamazepine normalizes activation and attenuates thermal hyperexcitability of sensory neurons due to Nav 1.7 mutation I234T. Br J Pharmacol 175:2261–2271.

Ye M, Yang J, Tian C, Zhu Q, Yin L, Jiang S, Yang M, Shu Y (2018) Differential roles of NaV1.2 and NaV1.6 in regulating neuronal excitability at febrile temperature and distinct contributions to febrile seizures. Sci Rep 8:753.

Yin L, Rasch MJ, He Q, Wu S, Dou F, Shu Y (2017) Selective modulation of axonal sodium channel subtypes by 5-HT1A receptor in cortical pyramidal neuron. Cereb Cortex 27:509–521.

Zhang J, Chen X, Eaton M, Wu J, Ma Z, Lai S, Park A, Ahmad TS, Que Z, Lee JH, Xiao T, Li Y, Wang Y, Olivero-Acosta MI, Schaber JA, Jayant K, Yuan C, Huang Z, Lanman NA, Skarnes WC, Yang Y (2021) Severe deficiency of the voltage-gated sodium channel NaV1.2 elevates neuronal excitability in adult mice. Cell Rep 36:109495.